PRS-JST-90-019
0 APRIL 1990

FOREIGN
BROADCAST
INFORMATION
SERVICE

JPRS Report

Science & Technology

Japan

3RD MICROELECTRONICS SYMPOSIUM

JPRS-JST-90-019
20 APRIL 1990

SCIENCE & TECHNOLOGY
JAPAN

3RD MICROELECTRONICS SYMPOSIUM

43067199 Tokyo MES'89 in Japanese 17-18 Jul 89 pp 1-245

[Selected papers presented at the 3rd Microelectronics Symposium held 17-18 July 1989 in Tokyo]

CONTENTS

Activated Metal Junction Technology for AlN/Cu System High-Power Module Substrate

4306/199A Tokyo MES'89 in Japanese 17-18 Jul 89 pp 11-14

[Article by Tsuneo Kawauchi, et al., Showa Denko K.K.]

[Text] Junction conditions, quality characteristics and especially the micro hair cracks of ceramics as occurring in a shock resistance test have been investigated in detail in regard to the junction technology of Al_2O_3 and AlN substrates with copper by the activated metal method. Cracks are caused by the tensile stress extended to ceramics which is brought about by the difference in thermal expansion coefficients between copper and ceramics. Factors for improving crack resistance, such as 1) junction strength, 2) copper plate thickness, and 3) the physical properties of ceramics, have an effect, while improving the mechanical strength of ceramics is especially important and quality stabilization is desired.

1. Introduction

Various new materials have been appearing in recent years. Research on composite materials, in which metals are combined with ceramics, utilizing their mutual advantages, has been actively promoted so that the right material can be used in the right place.

We have promoted research on junction technology based on compositing by paying attention to the phenomenon occurring in the interface. In this research, we have mainly used the activated metal method and have developed a process in which the junction of various metals and ceramics is possible on a mass production scale.

In this report, an explanation will be given of the electronics composite substrate material "Alcosink," which makes the most of both advantages—the superior electroconductivity and thermal conductivity possessed by copper, and superior electric insulating property possessed by ceramics.

Alcosink has both a high thermal conductivity several times that of alumina and a thermal expansion characteristic close to that of a semiconductor chip, and has been attracting particular attention in recent years. Alcosink is

comprised of the AlN/Cu system using an AlN substrate and the Al_2O_3/Cu system using an Al_2O_3 substrate.

Next we will explain the relationship between the junction technology and quality characteristics of both substrate materials when employing the activated metal method, and then the characteristics of Alcosink.

2. Junction Technologies by the Activated Metal Method

A rough classification of the junction technologies of metals and ceramics is given in Figure 1.[1]

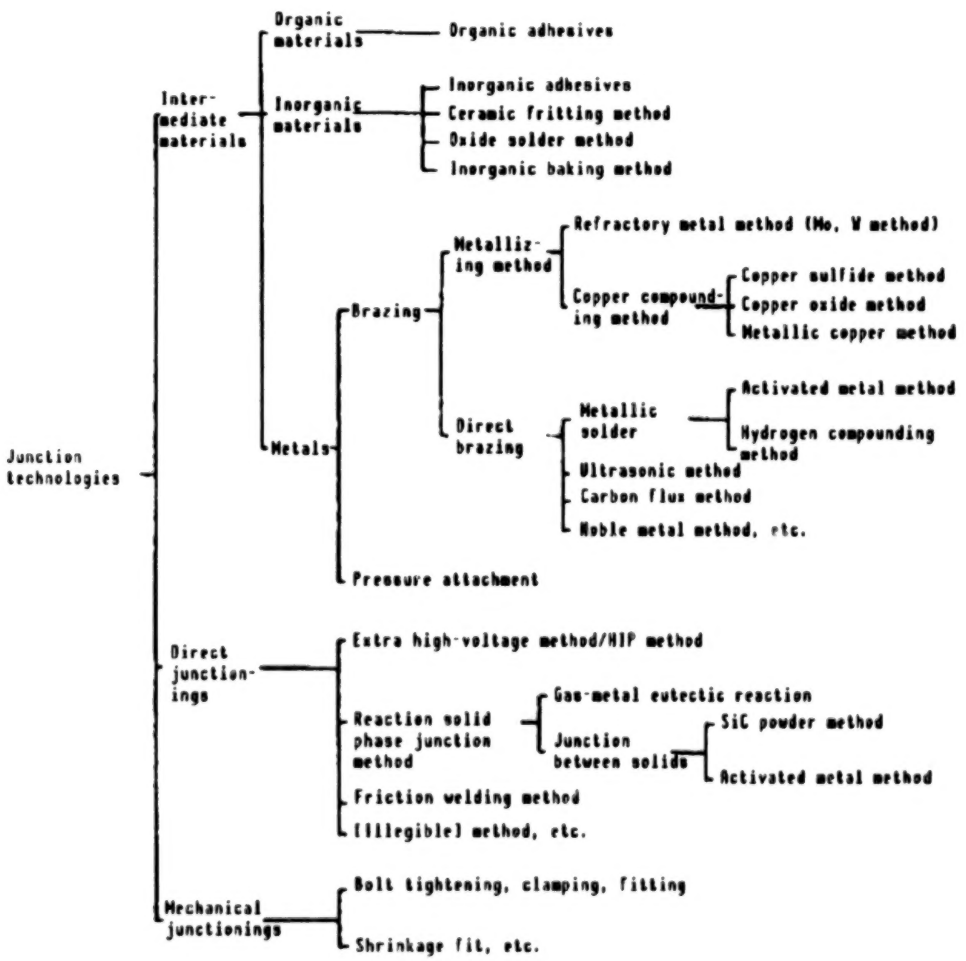

Figure 1. Junction Technologies of Metals and Ceramics

Among these junction thermal conductivity, the refractory metal method developed by Pulfrich[2] of West Germany has been greatly developed industrially and is currently being widely used. After metallizing the alumina surface with refractory metals, such as Mo and W, this method provides a plating and conducts brazing with metal. However, with the promotion of the high electrification and integration of power devices, the calorific value per unit area

of the substrate has also increased and the metallized substrate of the refractory metal method has already reached its limit in terms of use from the standpoint of radiation properties.

In addition, a mass production technology for use with the metallizing method of the AlN substrate, in which high heat conductivity is involved, has not yet been established.

As a substrate to replace the AlN substrate, Burgess, et al., of the United States has proposed the eutectic which conducts the junctioning of alumina substrates and copper by utilizing the eutectic point of copper and oxygen. A mass production technology based on this patent was developed by Iwase, Anzai, et al.,[4] however, there was a problem involving the thermal shock resistance and practical use was limited to a narrow range. In addition, the formation of an Al_2O_3 coating on the AlN surface is required, and it is feared that the intended high heat conductivity will be impeded when junctioning copper to the AlN substrate by means of the eutectic reaction method.

The activated metal method conducts junction by utilizing the reaction at the interface of refractory metals (Ti, Zr, Nb, Ta, etc.) and ceramics active against oxygen and nitrogen.[5] In the junction mechanism, the activated metals selectively disperse on the ceramic surface, form Ti oxide and TiN, and generate a junction by means of a mutual dispersion reaction. In conventional activated metal methods, an alloy foil, used as the insert material, was arranged in the middle of the junction material after being processed to the prescribed shape, and joining under a high load was adopted; however, when high reliability was demanded, a multilayer film was formed at the junctioning part by sputtering or vacuum deposition and then high load joining was adopted. The greatest disadvantage of these technologies lies in the fact that they cannot be used in mass production.

Our method uses Cu and Ag to control the junction temperature and junction interface wetness, and Ti is used as the activated metal. The greatest advantage is that the printing technology can be utilized since the insert material can be pulverized and used as a paste, and it excels in mass productivity. The production process diagram is shown in Figure 2. After processing the copper plate to the prescribed shape, the insert material is printed, positioning is made at the top and bottom of the ceramic substrate and junction is conducted at 850°C in the inert gas atmosphere under a high vacuum.

A mounting example of the AlN/Cu system power module substrate produced by this method and the semiconductor chip is shown in Figure 3.

3. Junction Technology and Reliability Test

The biggest problem we encountered during the development process involved improving reliability, and we concentrated our efforts on improving the thermal shock resistance. Topics included the generation of micro hair cracks in ceramics due to the difference in thermal expansion coefficients between silver and ceramics, and the rupture on the substrate due to the growth of micro hair cracks. The heat-resisting impact test was set to 150°C x 30 minutes

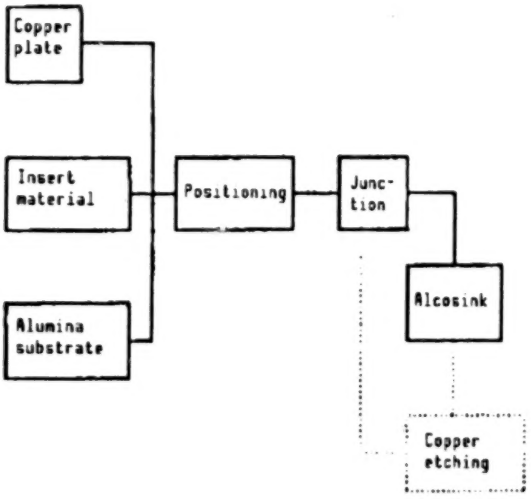

Figure 2. Alcosink Production Process Diagram

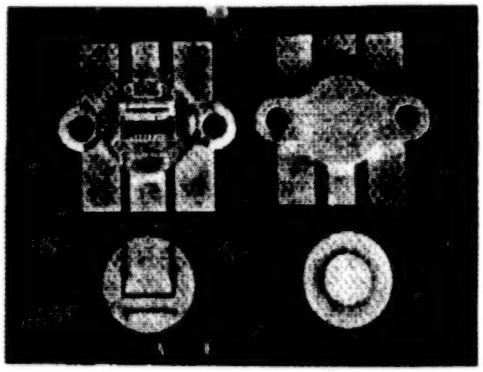

Figure 3. AlN/Cu System Power Module Mounting Substrate "Alcosink"

on the high temperature side and to −55°C x 30 minutes on the low temperature side, proof stress was applied repeatedly, and the generation of micro hair cracks was inspected. The inspection could not be conducted externally. Therefore, the red check method, the most exacting of inspecting ceramics, was adopted after etching copper with nitric acid in order to discover micro cracks.

3.1 Al_2O_3/Cu System Junction Conditions and Reliability Test

The relationship between the Ti concentration and junction strength in the insert material is shown in Figure 4. The junction strength was measured by the peel strength measuring method which peeled off the copper plate in the perpendicular direction at 90°C. It was ascertained that the junction strength rose rapidly with the increased Ti concentration.

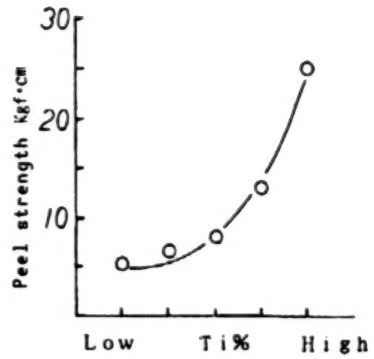

Figure 4. Relationship Between Ti Concentration and Junction Strength in Insert Material

The relationship between the junction strength and micro hair crack generation in the heat-resisting impact test is shown in Figure 5. It is conjectured that the higher the junction strength, the quicker the micro hair crack generation and the shorter the life of the substrate rupture. On the other hand, the copper plate peels off at the junction interface during the test and substrate rupture occurs due to insufficient strength when the junction strength is less than 2 kgf·cm. When the junction strength necessary for practical use is about 5 kgf·cm, peeling of the copper plate at the junction interface will not occur. Moreover, since the micro hair crack resisting life also improves, it is important to control the junction strength by the insert material composition and other junction conditions.

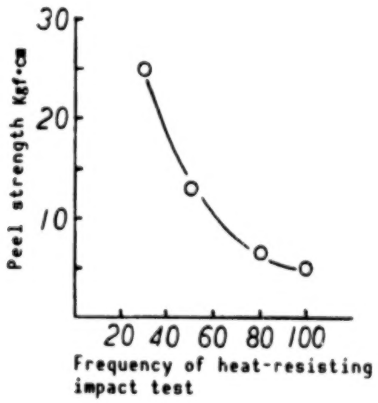

Figure 5. Relationship Between Junction Strength and Micro Hair Crack Generation

Results of investigating the effects of various companies' Al_2O_3 substrate materials on micro hair cracks and substrate ruptures are shown in Figure 6. Testing was conducted with all junction strengths fixed at 5~7 kgf·cm. It was ascertained from the diagram that the effect of the Al_2O_3 substrate material cannot be ignored either. Particularly, when making a detailed observation of the starting point of micro hair crack generation, it was determined that all cracks had generated from the Al_2O_3 intergranular and that such effects as the physical properties and strength of the substrate itself played an important role.

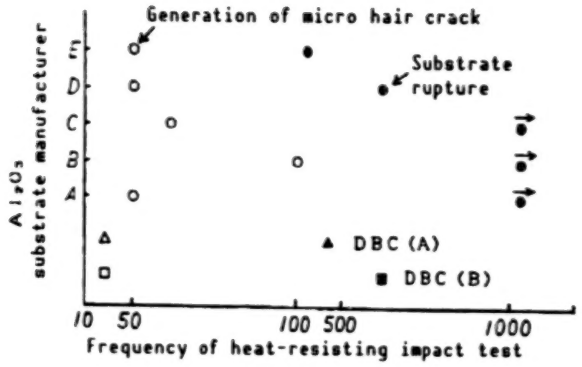

Figure 6. Relationship Between Al_2O_3 Substrate Material and Crack Resistance•Fracture Resistance

Figure 7 shows the results of investigating the copper plate thickness effect. The circuit side copper plate thickness was fixed at 0.3 mm^2 and the effect of the heat sink side copper plate thickness was investigated as a requisite of the high power module substrate. It is known from the diagram that the copper plate thickness effect is extremely great. The thinner the copper plate, in which the coefficient of cubic expansion becomes smaller, the more difficult it is for cracks to generate and the slower the growth rate becomes. In the crack generation mechanism, cracks generate directly under the convex part of the copper pattern where the greatest tensile stress is concentrated due to the thermal expansion coefficient difference, and cracks grow toward the linear part of the pattern because of the repeated stress. These results coincide well with the computer simulation results.

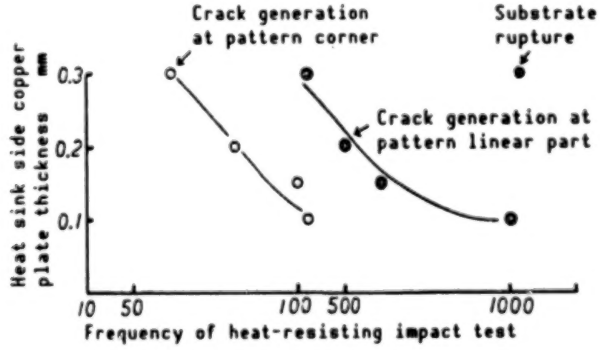

Figure 7. Relationship Between Heat Sink Side Copper Plate Thickness and Crack Resistance

It is difficult to use the above results to totally prevent the generation of micro hair cracks, however, the following measures are effective:

1) Control junction strength
2) Select Al_2O_3 substrate material
3) Thin plating of heat sink side copper plate

It is thought necessary for these measures to be reflected in the design stage.

3.2 AlN/Cu System Junction Conditions and Reliability Test

It is indispensable that the copper-oxygen eutectic reaction method in the AlN/Cu junction form an Al_2O_3 coating on the AlN surface to secure the oxygen source. In contrast, the activated metal does not require an Al_2O_3-izing treatment during junctioning because the reaction at the interface with AlN is utilized and junctioning is possible without marring the AlN substrate. In addition, it enables the Ti concentration in the insert material to be controlled freely, allowing its characteristics to coincide with the characteristics demanded by the users.

Figure 8 shows the relationship between the Ti concentration in the insert material and junction strength (peel strength).

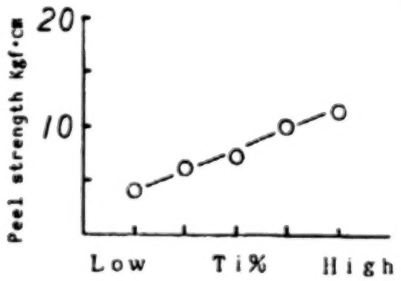

Figure 8. Relationship Between Ti Concentration and Junction Strength in Insert

Specifications of AlN substrate as given by catalog characteristic values of various companies are shown in Table 1.

Table 1. Characteristic Value of AlN Substrate of Various Companies

	A	B	C	D	E	F	G	H
Density (g/cc^3)	3.3	3.3	3.30	3.25	3.29	3.2	3.26	3.3
Hardness (HV)	1100	1100	1100	1100	--	1200	--	1100
Bending strength (kg/mm^2)	35	35	30~40	30~40	30	30	45	40
Thermal conductivity (W/m·X)	170	70	180	170	160	160	180	130
Thermal expansion coefficient ($x10^{-6}/°C$)	4.6	4.6	4.4	4.4	4.3	4.3	3.9	4.8
Volume resistivity (Ωcm)	10	10	10	10	10	10	10	10
Dielectric constant (1 MHz, RT)	8.8	8.8	9.2	8.9	8.9	8.9	8.5	8.7
Withstand voltage	15	14	15	15	15	30	30	
Tan δ ($x\ 10^{-4}$, 1 MHz)	5	10	5	5	3	5	5	4

Figure 9 shows the relationship between the AlN substrate of various companies when junctioned under optimum conditions in accordance with the standard specifications of Showa Denko and the generation of micro hair cracks from a heat-resisting impact test. Although great differences in physical properties

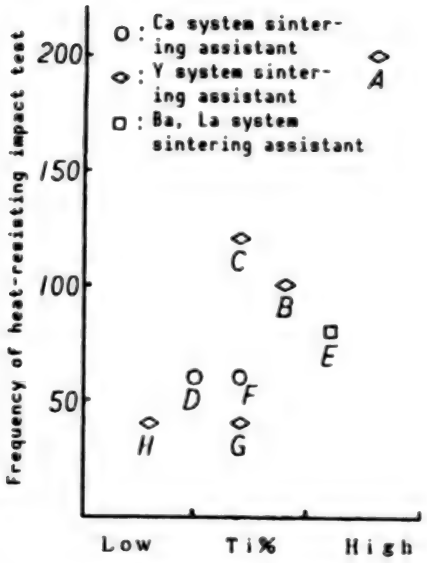

Figure 9. Optimum Junction and micro hair crack Generation of AlN Substrates of Various Companies

were not recognized in the AlN substrates of various companies from the catalog characteristic values, the heat-resisting impact characteristics were actually quite disparate.

Therefore, an actual survey of the bending strength of AlN substrates of various companies was made, and the results of an investigation of its relationship with micro hair crack generation is shown in Figure 10. It is recognized that the bending strength of the AlN substrate in particular exerts an extreme effect on crack generation. The AlN/Cu system Alcosink, with characteristics equivalent to those of Al_2O_3, has already been marketed. However, special care is necessary in the selection of substrate materials, and high quality stabilization of the substrate is desired.

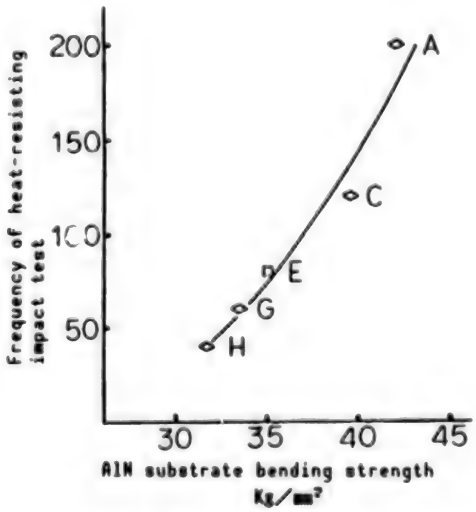

Figure 10. Relationship Between Bending Strength and Micro Hair Cracks of AlN Substrate

4. Characteristic of High Power Module Substrate Alcosink

Alcosink has the following characteristics:

(1) Since it has a structure close to that when junctioning the copper circuit board directly to the ceramic substrate, it has an excellent heat-dissipating property and characteristics approach those of BeO, especially in AlN.

(2) Both the mounting process and the structure can be simplified when compared with the metallized substrate generated by the refractory metal method.

(3) High frequency loss is small, and a large electric current is possible.

(4) Its heat-resisting impact property is excellent.

The general characteristics of Alcosink are shown in Table 2, and a comparison of the characteristics of various high heat-dissipating property substrates of the Al_2O_3 system are shown in Table 3.

Table 2. General Characteristics of Alcosink

Ceramic substrate	Al_2O_3	AlN
Purity (%)	96	>99
Insulation pressure proof (KV/mm)	10	15
Dielectric constant (1 MHz)	8.5	8.8
Young's modulus (10^4 kg/mm)	3.7	3.2
Bending strength (kg/mm)	25	30~40
Thermal expansion coefficient (10^{-6}/°C)	7.3	4.5
Thermal conductivity (W/m·K)	20	70~170
Alcosink	**Cu/Al_2O_3**	**Cu/AlN**
Al_2O_3 plate thickness (mm)	0.635	0.635
Cu plate thickness (mm)	0.3	0.3
Pattern width (mm)	0.5	0.5
Breakdown voltage (AC·KV)	>2	>2
Interfacial roughness R_{max} (μm)	<5	<5
Solder wetness	superior	superior
Hydrogen brittlement	nil	nil
90° peel strength (kg·cm)	>5	>5
Vertical tensile adhesion strength (kg/cm^2)	>100	>100
Heat-resisting impact test (-55°C ⇌ +150°C)	>100 cycles	>100 cycles
(DBC substrate)	<30 cycles	<30 cycles

Table 3. Characteristics of Various High Heat-Dissipating Property Substrates

	Alcosink		Refractory metal method
Junction method Junction temperature	Activated metal method 850°C	Cu-O eutectic method 1065-1083°C	Telefunken method 1400-1600°C
Heat-resisting impact property Heat resistance	More than 100∞ ● 2.95°C/W ●	20-30∞ Δ 3.02°C/W ●	More than 200∞ ● 4.10°C/W Δ
Large electric current realization Hydrogen brittlement Mounting density	● ● ●	○ x ●	x ● x

Alcosink is optimum for the mounting of large electric current, high voltage, and high frequency semiconductors by making the most of its characteristics. In addition, application expansion to structural materials, taking full advantage of wear resistance, corrosion resistance, and high temperature characteristics, is also being promoted. We look forward to the increasing development of this technology.

References

1. Suzumori, Iwase and Sugiura, JAPAN MACHINERY SOCIETY MAGAZINE, Vol 8 No 6, 1986, p 590.

2. Takashio, JAPAN METAL SOCIETY REPORT, Vol 24 No 2, 1985, p 113.

3. Burgess, J.F., et al., SOLID STATE TECHNOLOGY, May 1975, p 42.

4. Anzai, Iwas and Sugiura, TOSHIBA REVIEW, Vol 39 No 8, 1984, p 500.

5. Arakawa and Omori, JAPAN WELDING SOCIETY MAGAZINE, Vol 52 No 8, 1983, p 624.

6. Soji, Kawauchi, et al., JAPAN METAL SOCIETY REPORT, Vol 27 No 5, 1988, p 379.

7. Soji and Sekida, Electronic Information Communication Society, CPM87-35, 1987.

8. Soji, Kawauchi and Sekida, Micro Junction Research Committee, MJ-93-88, 1988.

Application of Aluminum Nitride to Large Electric Power Insulating Substrate

43067199B Tokyo MES'89 in Japanese 17-18 Jul 89 pp 15-18

[Article by Shinichi Iwata, Tokin Co., Ltd.]

[Text] The application of aluminum nitride (AlN) as a material with both superior thermal conductivity and insulating properties has been promoted mainly for use in semiconductor substrates. Since studies of the plating process of AlN substrates have been conducted, a 100 μm-thick copper circuit-provided substrate has been developed, and this substrate has been put to practical use as an insulating high-frequency SIT power module substrate, they will be reported here.

1. Introduction

Amid the promotion of high integration and large power realization as applied to mounting elements, the demand for a circuit substrate of high thermal conductivity aluminum nitride has increased.

Studies are being promoted on the following two methods for regenerating a copper circuit pattern on the aluminum nitride surface have been attempted.[1,2] However, handling the thermal strain caused by high temperature processing and forming a micro wiring pattern become problems.

The plating method has the advantages that the thermal stress during processing is small and correspondence up to those of a micro pattern size is possible as well as being cheap, and studies are also being partially promoted on aluminum nitride.[3,4]

Together with reporting the formation of a copper circuit with a thickness of 100 μm and the obtaining of a substrate with a stable film adhesion strength of more than 2 kg/mm^2 through plating process studies, such as surface roughening treatment, heat treatment conditions, etc., of the AlN substrate, we will report on the effect resulting from putting this substrate to practical use as a power module substrate.

2. Experimental Method

2.1 AlN Substrate

Studies were conducted using the AlN substrate manufactured by Tokin Co. The substrate characteristics are shown in Table 1 in comparison with those of the Al_2O_3 and BeO substrates.

Table 1. Comparison of Characteristics of AlN Substrate and Al_2O_3, BeO Substrate

Characteristic	Tokin AlN	Al_2O_3 (96.0%)	BeO (99.5%)
	T-200		
Density (g/cm^3)	3.2	3.8	2.9
Thermal conductivity (W/mK (RT))	200	20	260
Thermal expansion coefficient ($x10^{-6/°C}$) (RT~400°C)	4.3	6.7	7.5
Insulation pressure proof (KV/mm (RT))	15	15	10
Specific resistance (Ω·cm (RT))	>10°	>10°	>10°
Dielectric constant (1 MHz, RT)	8.9	8.9	6.7
Dielectric loss (1 MHz, RT)	3	4	3
Deflection strength (kgf/mm^2)	30	30	25
Vickers hardness (kgf/mm^2)	1,200	2,000	1,200

The AlN substrate has a thermal conductivity coefficient of 200 W/mk, and its surface roughness had been adjusted to Ra=0.6 μm and thickness to 0.635 mm in advance by the abrasive machining method when studying plating.

2.2 Plating Film Formation

An outline of high power module substrate processing by plating is shown in Figure 1.

(i) The AlN substrate is immersed in a surface roughening treatment wave of 1N-NaOH (40°C), and surface roughening is conducted in the etching time range of 0~60 minutes. The changes in the substrate roughness and surface were checked by SEM in this case.

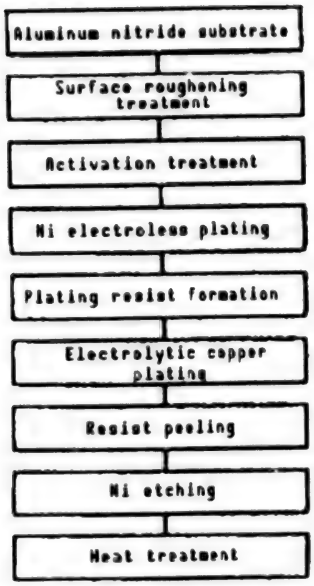

Figure 1. High Power Module Substrate Process Diagram

(ii) Electroless plating was conducted while forming a thick adhesion copper film for relaxing the stress between the AlN substrate and copper film and to improve the adhesion strength of the copper film.

The thickness was adjusted to 5 μm by an Ni-P marketed bath (pH 6.5, 70°C).

The AlN substrate only was dissolved in a heated NaOH solution so that the adhesion conditions between the Ni film and AlN substrate could be observed and, after the separation of the Ni film, SEM observation was made from the adhesion interface side with the substrate.[3] In addition, after soldering a 0.7 mm lead wire to a 2 mm^2 pad, the adhesion strength was evaluated by the vertical tensile strength.

(iii) Formation of the plating resist employed a liquid resist and the printing method.

(iv) Thick adhesion copper plating, 100 μm thick, was generated under an electric current density of 2 A/cm^2 at room temperature by using a sulfuric acid copper plating bath for the electrolytic copper plating.

(v) The resist was removed after the plating film formation, and pattern formation was conducted by removing the Ni film from unnecessary places through etching.

(vi) Heat treatment for stabilizing the plating film was conducted for an hour each at various temperatures ranging from room temperature to 600°C, and the relationship between the adhesion strength evaluation of the film and the hardness of the Ni film substrate was checked.

3. Results and Discussions

3.1 Surface Roughening Treatment and Adhesion Strength

The relationship among the etching time, surface roughness and adhesion strength of the Ni film by surface roughening treatment is shown in Figure 2.

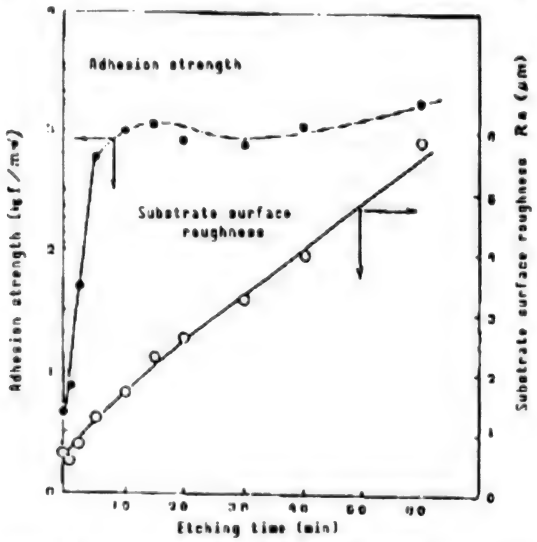

Figure 2. Relationship Among Etching Time, Density Strength and Substrate Surface Roughness of AlN Substrate

The surface roughness of AlN substrate increases in proportion to the etching time by 1N-NaOH.

The adhesion strength of the Ni film shows a sudden increase up to the approximate surface roughness of Ra=1.5 μm, reaching 3 kg/mm^2. However, an increase in the adhesion strength generally does not occur after this, even when surface roughening progresses, settling somewhere around 3 kg/mm^2.

The etching conditions (0-10 minutes) of the AlN substrate by NaOH are shown in (A-1) to (A-3) of Photo 1 [not reproduced], while conditions of the Ni film adhesion surface corresponding to the substrate are shown in (B-1) to (B-3) of Photo 1 [not reproduced].

The falling of crystal grains resulting from abrasive machining is observed in the AlN substrate surface at 0 minute etching, but intergranular erosion is not observed. The corresponding Ni film surface also adopts an intermittent shallow net structure only in a form running parallel with the AlN crystal grains (A-1 and B-1 of Photo 1 [not reproduced]).

The surface processing layer is removed and etching of the crystal grain triple point and intergranular occurs in the AlN substrate at 1 minute etching. The net structure of the Ni film is formed continuously over several layers (see A-2 and B-2 of Photo 1 [not reproduced]). After an elapse of 10 minutes, the intergranular of the AlN substrate is firmly etched and etching of the surface layer crystal grains is also promoted. The net structure of

the Ni film becomes thick and dense, and a high value of approximately 3 kg/mm^2 is obtained for the adhesive strength (see A-3 and B-3 of Photo 1 [not reproduced]).

Although surface roughening is augmented after this, further depression of the AlN surface layer causes surface roughening, but great changes in the film net structure do not occur.

These phenomena suggest a relationship between the film adhesion strength and net structure.

3.2 Heat Treatment and Adhesion Strength

The relationship between the heat treatment temperature and plating adhesion strength is shown in Figure 3.

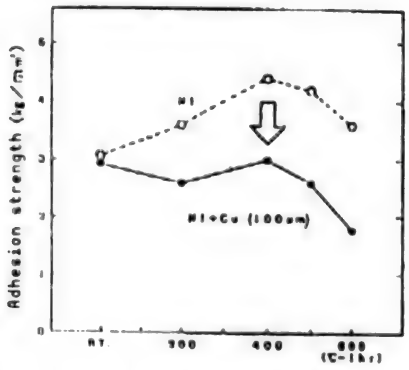

Figure 3. Heat Treatment Temperature and Plating Film Adhesion Strength

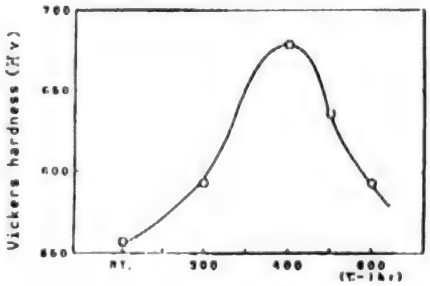

Figure 4. Heat Treatment Temperature and Ni Plating Film Hardness

When heat treatment of 1 hour is conducted at various temperatures up to 600°C after Ni plating to a 5 μm thickness, the adhesive strength of the film is greatly improved, from 3.1 kg/mm^2 before treatment to 4.4 kg/mm^2 at 400°C treatment.

The adhesion strength, however, drops when a copper plating 100 μm thick is provided after the Ni film formation, and a strength of 3.1 kg/mm^2 was ultimately obtained at 400°C treatment. This value does not impede practical use.

These phenomena coincide well with the hardening phenomena by heat treatment in Ni-P electroless plating.

Figure 4 shows the relationship between heat treatment and the hardness of the Ni plating film used in this experiment. Film hardness becomes the greatest at around 400°C. This is believed to be attributable to the crystallization of the Ni particles and precipitation hardening of nickel phosphide (Ni_3P).[5]

From the matters mentioned above, the film adhesion strength mechanism can be thought of as follows:

(1) The more the net structure of the Ni plating is developed along the etched AlN intergranular, the more an increase in the adhesion strength can be promoted by the anchor effect. However, a sufficient etching that does not cause the falling of AlN crystal grains becomes necessary.

(2) A stronger net structure is generated by Ni hardening when further heat treatment is provided and adhesion strength is improved.

(3) After this, the two effects mentioned above will be inherited when a thick adhesion plating of copper is provided, but the adhesion strength will drop due to the thermal strain between the Ni and Cu films. A final adhesion strength of 3.1 kg/mm^2 (400°C treatment) is available.

3.3 Reliability Evaluation

After forming a copper film 100 μm in thickness, a heat cycle test (MIL-STD883-1010-C, -65°C~150°C) was conducted on 400°C heat treated items and nontreated items, and the results are shown in Figure 5.

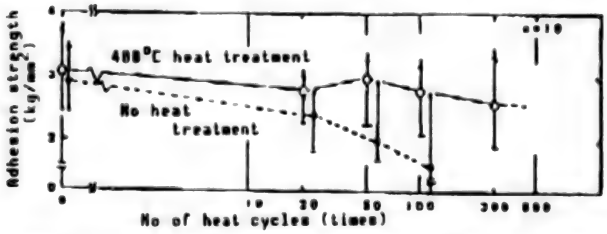

Figure 5. Heat Cycle Test MIL-STD883-1010-C (-65°C·——·150°C)

The adhesion strength becomes less than 2 kg/mm^2 at more than 50 cycles for nontreated items, and they cannot be used for practical use. Items heat treated at 400°C, however, exhibited an adhesion strength of 2.5 kg/mm^2 at 300 cycles, and it has been confirmed that they are extremely stable when exposed to severe temperature cycles.

4. Application to High Power Module Substrate

An insulating-type high-frequency SIT power module of the rated 600V-30A class mounting an AlN substrate has been developed based on the results mentioned above, and a comparison of the structure and heat-dissipating effect between the Al_2O_3 substrate and a conventional metal flat base package type has been made.

The appearance and internal structure of the developed insulating type module and the comparison with the conventional metal flat base package type are shown in Photo 2 [not reproduced]. In addition, the structural cross sections of the respective modules are shown in Figure 6.

Since the conventional metal flat base package necessitated an electric insulating sheet in order to obtain electrical insulation with the package body for use in mounting, it resulted in an increase in the number of parts, as well as an increase in thermal resistance for mounting. On the other hand,

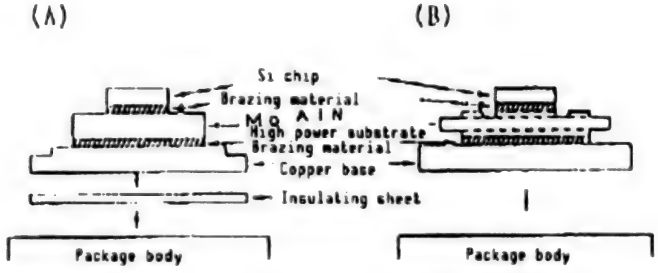

Figure 6. Cross Section of High Frequency SIT Power Module Structure

a reduction in the number of parts and the simplification of the structure could be promoted in the insulating type module when the AlN substrate was used. This effect becomes more conspicuous when trying to mount multiple elements on the substrate.

The measured results of the area of safety operation (ASO) of the module is shown in Figure 7. The solid line shows the case of the insulating-type module using an AlN substrate, while the broken line shows a metal flat base package (thin line) with an intervening electrical insulating sheet (thermal resistance 0.3°C/W, thickness 0.3 mm) (thick line). In addition, the insulating-type module using an Al_2O_3 substrate is shown by a single dotted line. It was ascertained from the heat-dissipating effect that the ASO expansion had been promoted to two times that when using the Al_2O_3 substrate and 1.1 times that of the metal package-type when mounted to the package body in an SIT insulating-type module using an AlN substrate. As a result, the effectiveness of the AlN high power module substrate has been confirmed.

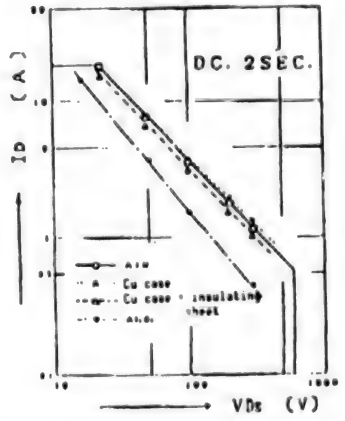

Figure 7. Effect Substrate Exerts on Area of Safety Operation (ASO)

In addition, it has also been confirmed that it was superior in regard to solder wetness and wire bonding properties when mounting an SIT chip of an AlN high power module substrate, and no problems involving practical use were found.

5. Conclusion

The topics mentioned above have been arranged as follows:

1. A copper film, 100 μm thick, has been formed, and superior heat cycle properties (-65~150°C, more than 300 cycles) and adhesion strength (2.5 kg/mm^2) have been obtained by studying the application of the thick adhesion plating process to an AlN substrate.

2. Application has been made to the AlN high power module substrate and it has been confirmed that there are no problems in practical use.

3. As a result of applying the substrate mentioned above to the insulating-type module, ASO improvement, parts reduction, and structure simplification have been confirmed.

(This module has been put to practical use in Tokin Co. as a high-frequency SIT power module with a proven pressure of 450-1000 V, I_D = 30 A and ft = 50 MHz.)

Note of Appreciation

We are very grateful that a portion of this experiment was financed by the Basic Technology Research Promotion Center.

References

1. Iwase, N., et al., IET Transactions, CHMT-8, No 2, 1985, p 253.

2. Soji, Kawauchi, Sekida and Kashima, JAPAN METAL SOCIETY REPORT, Vol 27 No 5, 1988 p 379.

3. Osaka, T., Asada, T. and Nakajima, et al., J. ELECTROCHEM. SOC., Vol 133, 1986, p 2346.

4. Ibid., Vol 135, 1988, p 2573.

5. Tokyo Plating Material Cooperative Association Technology Committee, "Plating Technology Guidebook," p 316.

Degree of Sintering, Thermal Conductivity of Aluminum Nitride Ultrafine Particles

43067199C Tokyo MES'89 in Japanese 17-18 Jul 89 pp 19-22

[Article by Yumi Aikawa, et al., Nippon Electric Co., Ltd.]

[Text] High purity AlN ultrafine particles were obtained by directly nitriding metallic aluminum with ammonium by the radio frequency heating plasma method (RF plasma method). The particle diameters of ultrafine particles were 200-600 Å, less than one-tenth that of conventional particles, and metallic impurities were less than one-half. In addition, the degree of sintering was remarkably improved, with a sintered material having a thermal conductivity coefficient of 110 W/m·K, which is about six times that of alumina, being obtained at the low sintering temperature of 1400°C.

1. Introduction

Since aluminum nitride (AlN) has a high mechanical strength, exhibits high insulating properties, and the theoretical value of its thermal conductivity coefficient is 320 W/m·K and higher, R&D on aluminum nitride as a high thermal conductivity ceramic substrate material and heat sink material for LSI and high power devices have become active in recent years. AlN ceramics with a high thermal conductivity coefficient exceeding 260 W/m·K have already been developed. This value is still low in comparison to the theoretical value. Reasons for this are that AlN is difficult to sinter, it is difficult to obtain a perfectly precise sintered material unless its sintering temperature reaches about 2000°C, and the thermal conductivity coefficient value is strongly dependent on the impurity content, and particularly the oxygen, contained in the AlN.

This research was conducted for the purpose of developing high thermal conductivity coefficient AlN ceramics which would allow low temperature sintering by using high-purity ultrafine particle AlN. Various products have been manufactured up to now by conducting ultra-rapid quenching of vapor phase substances that had been heated and evaporated by a high temperature heat source during the production of ultrafine particles. The atmospheric operating RF plasma[2] developed by Reed in 1961 is extremely convenient for obtaining an ultrahigh temperature and clean environment. Since the RF plasma temperature reaches 10,000 K, the advantages include practically the entire

substance being evaporated and chemically-active types, such as ions, radicals and dissociation atoms, being generated and capable of being utilized. Therefore, this method is used for the synthesis of various substances as well as of ultrafine particles.[3-5] Reports will be made here on the method of synthesizing ultrafine particles by the RF plasma method, on powder characteristics and the degree of sintering, and on realizing the high thermal conductivity of sintered materials.

2. Experiment

2.1 Powder Synthesis

Figure 1 shows the schematic diagram of an RF plasma reaction system for synthesizing ultrafine grain powders. This system consists of the RF generator (13.56 MHz, 20 kW), plasma torch, reaction chamber, gas and raw material feeders, exhaust pump, ultrafine particle recovery filter, etc. The entire system produces exhaust up to about 10^{-2} Torr in advance and encloses Ar gas until it reaches atmospheric pressure. When plasma gas ($Ar-N_2$ mixed gas) is introduced from the upper part of the plasma torch and high frequency flows in the coil, a high temperature plasma flame is generated in the torch. A metallic aluminum powder (purity: 99.99 percent) and NH_3 gas were introduced into this plasma, and AlN synthesis was conducted by the following reaction:

$$2\ Al + 2\ NH_3 = 2\ AlN + 3\ H_2 \qquad (1)$$

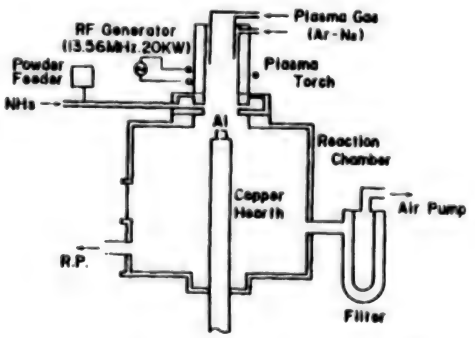

Figure 1. Schematic Diagram of an RF Plasma System

The AlN produced by the reaction in high temperature plasma is rapidly quenched in the reaction chamber and becomes ultrafine particles. The ultrafine particles produced are sent to the filter, together with the carrier gas, and recovered. Ultrafine particle AlN powder of more than 200 g/hr was obtained in this experiment when the Al powder input was 250 g/hr and the NH_3 gas flow rate was 20 ℓ/minute.

2.2 Evaluation

An evaluation was made by conducting X-ray diffraction, TEM (transmission electron microscope) observation, BET specific surface area measurement, ICP impurity analysis, IR measurement, NMR (nuclear magnetic resonator) measurement and oxygen measurement.

These ultrafine particles were formed by the rubber press method under normal pressure of about 2 ton/cm^2, and those sintered in an N_2 atmosphere were made the sintered samples. An evaluation of these samples was made by density measurement, X-ray measurement, thermal conductivity coefficient measurement, oxygen measurement, SEM (scanning electron microscope) observation, and EDX analysis.

3. Results and Considerations

3.1 Characteristics of Powder

There was no unreacted metallic aluminum residue in the powders following the powder X-ray diffraction and AlN was of a single phase. Figure 2 [not reproduced] shows a TEM photo of the AlN ultrafine particles, with a photo of AlN powders produced by the ordinary alumina reduction method shown for comparison. The particle shape is a hexagonal cylinder or a hexagonal plate, and it is a single crystal particle in which the crystal habit of the wurtzite structure AlN crystal is well expressed.

Table 1 gives the characteristics of this ultrafine particle AlN powder. The specific surface area is 30 m^2/g in the ordinary synthesizing condition, and the average particle diameter obtained from this is 60 nm. It is possible to control the average particle diameter of the particles to a certain extent by the synthesizing condition. Metal impurities totaled about 100 ppm, which was about one-half that obtained with conventional AlN powders. Since the main impurities of Si, Fe and Cu did not exceed the content contained in the metallic aluminum powders of the raw materials, it is thought that they resulted from the raw material powders. The atomic ratio of N/Al was 0.91~0.93. The nitrogen atom shortage will be mentioned later, but it is thought that this is due to a hydroxide layer being formed on the ultrafine particle surface. The impurity oxygen content was about 3 wt percent for a sample with a particle diameter of 60 nm. The oxygen content tended to increase approximately in proportion to the specific surface area when the powder remained in the air.

Table 1. Characteristics of Ultrafine Particles AlN Powder

Specific surface area	~30 $m^{2/g}$
Particle diameter	~60 nm
Metallic impurity content	~100 ppm
Impurity oxygen content	2~ 25%

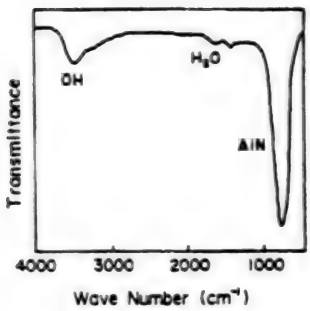

Figure 3. FT-IR Spectra of the Ultrafine Powder

Figure 3 shows an FT-IR spectra of the synthesized ultrafine powder.[6] Absorption by OH bonding is seen near the wave number around 3500 cm^{-1}, and weak absorption by moisture is seen near 1600cm^{-1}. It is thought that absorption by OH and moisture is due to the active ultrafine particle surface absorbing moisture in the air, and $Al(OH)_3$ is produced through the following reaction with AlN.

$$AlN + 3\ H_2O = Al(OH)_3 + 3\ NH_3 \qquad (2)$$

It is believed that moisture causes a weak bond to form on the $Al(OH)_3$ layer formed on the ultrafine particle surface due to Van der Waals force. This fact[2] has been confirmed by an experiment using H-NMR.[7] This impurity oxygen reacts with AlN during sintering and generates an acid nitrate in the sintered material, resulting in an extreme decrease in the thermal conductivity.[8] Therefore, it is necessary to conduct surface reforming, etc., so that the ultrafine particle surface does not react with moisture and to protect the surface when obtaining powder of low oxygen concentration.

3.2 Degree of Powder Sintering

Figure 4 shows the experiment results of the degree of sintering of three types of AlN with different particle diameters. Sintering was conducted for an hour in atmospheric N_2 from 1000°C to 1900°C without adding a sintering assistant. Those with particle diameters of 0.02 μm and 0.08 μm were synthesized by the RF plasma method, while all others used were commercial AlN powder prepared by the reduction method. As is clear from the diagram, the degree of sintering is strongly dependent on the particle diameter. It has already reached 3.26 g/cm^3 at 1600°C, practically attaining the theoretical density value, especially at ultrafine particles with particle diameters of 0.02 μm. In contrast to this, a sufficiently fine sintered material was not available for ordinary AlN powders, even at 1900°C.

Figure 5 [not reproduced] is an SEM photo of the fracture surface of samples sintered at 1400°C for 10 and 50 hours. Pores are observed on the sample sintered for 10 hours, but the number of pores had decreased in the sample sintered for 50 hours and it was ascertained that particle growth had taken place. It was previously said that it was difficult to realize a fine AlN under such a low temperature level, no matter what the additive, however, low temperature sintering has become possible for the first time by converting to ultrafine particles.

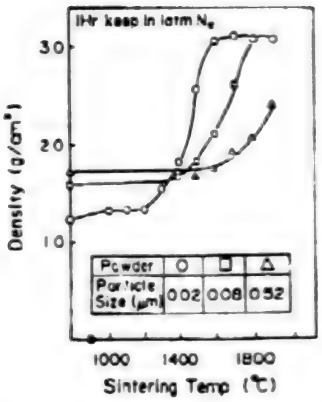

Figure 4. Densification Behavior of AlN Powders With Different Particle Sizes

3.3 High Thermal Conduction of Sintered Materials

The thermal conductivity value was about 100 W/m·K and not as high in a sintered material without an additive that had been sintered at 1900°C for 10 hours since the oxygen contained in the powder was great. There have been many reports regarding the effect of additives (sintering assistants) on realizing a high thermal conduction of AlN sintered materials. The role of additives is to form a different phase by reacting with the oxygen contained in AlN powder and to remove the oxygen from the interior of the sintered material by discharging this different phase to the system exterior.[9] As a result of testing by using various additives, it was ascertained that sodium fluoride (YF_3) was extremely effective for improving the thermal conductivity of the ultrafine particle AlN.[10]

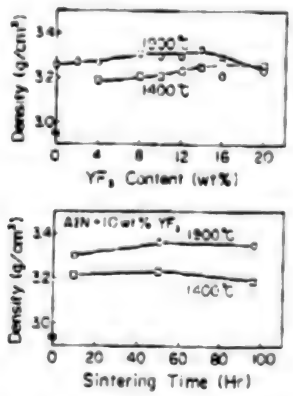

Figure 6. Density of AlN Ceramics Using Ultrafine Particles

Figure 6 shows the YF_3 and sintering time dependencies of sintering density. Ultrafine particle AlN does not become fine when sintered at 1400°C unless YF_3 is added, however, a fine sintered material of more than 98 percent was obtained at the low temperature of 1400°C by adding YF_3 of more than 4 wt percent. A fine sintered material was not available at 1400°C in an ordinary AlN powder, even when using an additive. As seen here, the sintering

temperature of ultrafine particle AlN could be lowered by about 500°C from that of ordinary AlN powder with an average particle diameter of 0.5 μm by using the YF_3 additive. The density exceeds the theoretical value at 100°C, but this is due to the Y-Al-N compound remaining in the sintered material.

Figure 7 plots the thermal conductivity against YF_3 content when the sintering conditions have been changed. A thermal conductivity of 220 W/m·K was obtained under the sintering conditions of 1900°C for 50 hours with the YF_3 content in the neighborhood of 8~10 wt percent. A thermal conductivity value of 110 W/m·K was also obtained under sintering of 1400°C for 50 hours, which means that a thermal conductivity of about five times that of alumina has been achieved at the same sintering temperature level as alumina. Thermal conductivity, as shown in Figure 7, increases with increases in the sintering temperature and sintering time. Thermal conductivity decreases when the YF_3 content exceeds 10 wt percent. This is thought to be due to the excessive additives remaining in the sintered material and impeding thermal conductivity. As a result of the SEM microstructure observation of samples to which 10 wt percent of YF_3 has been added, the average particle diameter of those sintered for 10 hours was 4~5 μm, with many intergranular phases existing. On the other hand, the average particle diameter of those sintered for 50 hours was 6~7 μm, with a reduced number of intergranular phases occurring in comparison to those sintered for 10 hours. The thermal conductivity for those undergoing 10-hour sintering was 180 W/m·K, while the thermal conductivity for those undergoing 50-hour structure was 220 W/m·K. It is deduced from this that a high thermal conductivity is achieved when the particle diameter is enlarged and the intergranular phases are removed.

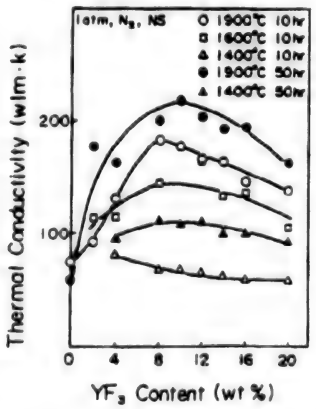

Figure 7. Thermal Conductivity of AlN Ceramics Using Ultrafine Particles

As we have mentioned previously, this shows that YF_3 is extremely effective for realizing both low temperature sintering and high thermal conductivity of ultrafine particle AlN. It is believed that these results are due to the following reasons.

Since the driving force behind sintering involves the reduction of the surface free energy, it is apparent that the degree of sintering of ultrafine particles with greater surface energy becomes better. In addition, since the

melting point of YF_3 is 1150°C, the surface of AlN particles is mainly surrounded by the melted YF_3 liquid at temperatures exceeding 1150°C, and liquid phase sintering is started. It is said that the driving force behind fining is generated by the capillary pressure of the liquid phase existing between the micro solid particulates during liquid phase sintering. The presence of microparticles is necessary in the sintering process, and these microparticles generate capillary pressure in inverse proportion to the capillary diameter. A high capillary pressure will be available for AlN sintering since it involves ultrafine particles, and it is believed that sintering under lower temperatures than usual has become possible due to liquid phase sintering. Actually, a considerable density increase is recognized under the temperature of from 1100°C to 1200°C. Y_2O_3 and CaO are normally used as the sintering assistants of AlN powder. However, the melting point of these sintering assistants is more than 2000°C, and a liquid phase with a reactivity with oxygen, etc., in AlN will not be available unless a 1900°C sintering temperature level is attained. Therefore, when Y_2O_3 and CaO are used as the sintering additives, it will be impossible for sintering to occur under low temperatures, e.g., 1400°C, when ultrafine particles are involved as well.

Intergranular deposition phases containing a great deal of Y were observed by SEM observation and in EDX analysis. These intergranular deposition phases, according to X-ray diffraction, were Y-Al-O compounds, such as Y_2O_3, $Al_5Y_3O_{12}$, etc. It can be considered from this that the YF_3 liquid had reacted with the oxygen impurity on the powder surface and had become a Y-Al-O compound. Since this compound trapped the oxygen in the intergranular, it is thought that the thermal conductivity of AlN was increased. In addition, the X-ray diffraction results of those sintered at high temperatures of about 1900°C showed that the foreign phase in the sintered material had disappeared when the content of the YF_3 added was suitable, and YN had deposited on the sintered material surface. It can be conjectured that the Y-Al-O compound on the sintered material was first nitrified and then removed with the repetition of the process involving the foreign phase in the sintered material interior being deposited and nitrified on the surface, with the N_2 concentration gradient as the driving force.

4. Conclusion

An ultrafine particle AlN of high purity was synthesized by directly nitrifying the metallic aluminum by the RF plasma method. The specific surface area of the powder obtained was 30 m^2/g under representative synthesizing conditions, and the content of metallic impurities was about 100 ppm and of extremely high purity. The degree of AlN sintering improved remarkably as the raw material particle diameter became smaller, and an easy degree of sintering capable of sintering also at 1500°C, that is lower by 400°C than the conventional AlN, was exhibited in ultrafine particles without the addition of a sintering assistant. The high value of 110 W/m·K was obtained as the thermal conductivity of the sintered material under the conditions of a sintering temperature of 1400°C and YF_3 10 wt percent addition, and the potential for an AlN ceramic substrate with a thermal conductivity at the practical use level being obtained by low temperature sintering has been

made clear. In the future, we hope to define the relationship between the oxygen content or crystal particle size in the sintered material and thermal conductivity, and also aim at low temperature sintering and high thermal conductivity by studying the ceramic production process appropriate for ultrafine particles.

References

1. Slack, G.A., J. PHYS. CHEM. SOLIDS, Vol 34, 1973, p 321.

2. Reed, T.B., J. APPL. PHYS., Vol 32, 1961, p 821.

3. Hollabaugh, C.M., Hull, D.E., Newkirk, L.R. and Petrovic, J.J., J. MATER. SCI. LETT., Vol 18, 1983, p 3190.

4. Vissokov, G.P., Manolova, K.D. and Brakalov, L.B., Ibid., Vol 16, 1981, p 1716.

5. Yoshida, T., Tani, T., Nishimura, H. and Akashi, K., J. APPL. PHYS., Vol 54, 1983, p 640.

6. Baba, K., Shohata, N. and Yonezawa, M., Proceedings of Eighth International Symposium on Plasma Chemistry, 1987, p 2034.

7. Hayashi, S., Hayamizu, K. and Yamamoto, O., JPN. J. APPL. PHYS., Vol 26, 1987, p 682.

8. Sakai, T. and Iwata, M., J. MATER. SCI. LETT., Vol 12, 1977, p 1659.

9. Kuramoto, N. and Taniguchi, T., Ibid., Vol 3 [sic], 1984, p 471.

10. Baba, K., et al., To be published.

Effect of Baking Pressure on AlN Sintering

43067199D Tokyo MES'89 in Japanese 17-18 Jul 89 pp 23-25

[Article by Hiroshi Makihara, et al., Fujitsu Laboratory Co., Ltd.]

[Text] Particle growth by long periods of baking, evaporation removal of intergranular phases and the utilization of the reducing atmosphere are studied for the fining of AlN and obtaining a high thermal conductivity. $CaCO_3$ has been added as the sintering assistant, a liquid phase of calcium aluminate has been formed, and the fining and high thermal conduction of AlN have been promoted by changing the baking pressure in this research. As a result, it has become clear that, in order to obtain a high thermal conductivity, the baking pressure shifted to the low pressure side as the content of the added $CaCO_3$ increased.

1. Introduction

Since aluminum nitride (AlN) excels in thermal conductivity and its thermal expansion is close to that of Si, it has attracted attention as a ceramic substrate material enabling the high density mounting of LSI devices.[1] However, AlN is difficult to sinter as a simple substance, and it becomes necessary to bake at high temperature and pressure or to add sintering additives, such as Y_2O_3 and CaO, to obtain fine sintered materials.[2,3] In addition, the method of conducting a long period baking,[4] removing intergranular phases by evaporation and utilizing the reducing atmosphere[5] has been considered in order to improve the thermal conductivity.

In this research, $CaCO_3$ was added as the structure additive and a liquid phase of calcium aluminate ($Ca_xAl_yO_z$) was formed in order to promote the thermal conductivity of AlN, and the effect of the baking pressure exerted on liquid phase evaporation was studied.

2. Experimental Method

2.1 Preparation of Sample

AlN powder with an average particle diameter of 1.8 μm and oxygen content of 0.8 percent produced by the alumina reducing process was used for the raw material powder. $CaCO_3$ powder with an average particle diameter of 1.15 μm was

used as the sintering additive. The content of the sintering additive was made 2–8 wt percent by CaO conversion. These powders were kneaded with an organic binder solvent and formed into green sheets by the doctor blade method. These green sheets were laminated after having been cut to 15 mm^2, and they were degreased in a nitrogen ventilating current. Then, the pressure in the furnace was made 1–8 kg/cm^2 and the sintered material was prepared by baking for 9 hours at 1900°C in the nitrogen ventilating current.

2.2 Evaluation

The calcium content remaining in the sintered material was measured by fluorescent x-rays, and the residual oxygen content was measured by the infrared absorption method. The sample was abrasive machined to 10ϕ x 3 mm, and thermal conductivity was measured by the laser flash method. In addition, the abrasive machined surface of the sample was analyzed in the 100 μm range by micro section X-ray diffraction, and the rupture surface of the sample was observed by SEM.

3. Results and Discussions

3.1 Residual Calcium and Oxygen Content

The relationship between the residual calcium content in the sintered material and the baking pressure is shown in Figure 1. The residual calcium content is about 0.05 percent and low under a baking pressure of 1 kg/cm^2 (atmospheric), irrespective of the $CaCO_3$ addition content. The residual calcium content becomes fixed in AlN with the addition of $CaCO_3$ 2 wt percent by CaO conversion, irrespective of the baking pressure, but the residual calcium content increases from the baking pressure of 4 kg/cm^2 in AlN to which 4 wt percent and 8 wt percent of $CaCO_3$ has been added and, the greater the $CaCO_3$ content, the greater the residual calcium content.

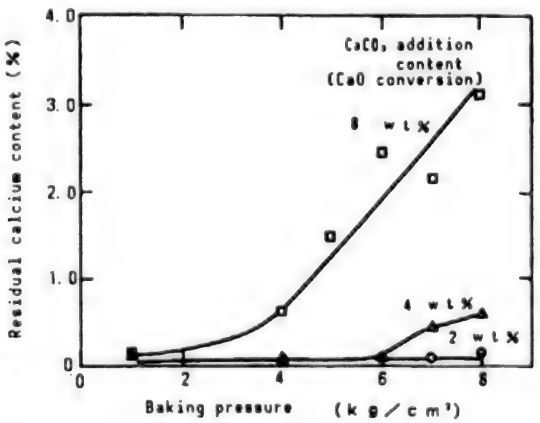

Figure 1. Relationship Between Residual Calcium Content and Baking Pressure in Sintered Material

The relationship between the residual oxygen content in the sintered material and the baking pressure is shown in Figure 2. Similar to the residual calcium

content, the residual oxygen content is around 0.2 percent and low in atmospheric baking, irrespective of the content of added $CaCO_3$. The residual oxygen content increases from the baking pressure of 4 kg/cm^2 in AlN to which 4 wt percent and 8 wt percent of $CaCO_3$ had been added and, the greater the added content, the greater the residual oxygen content.

3.2 Thermal Conductivity and Micro Section X-Ray Diffraction

The relationship between thermal conductivity and baking pressure is shown in Figure 3. The maximum value of thermal conductivity shifts to the lower baking pressure side as the added content of $CaCO_3$ increases. As shown in Figures 1 through 3, thermal conductivity becomes maximal at the low pressure side when compared to the baking pressure in which the residual calcium and oxygen contents increase.

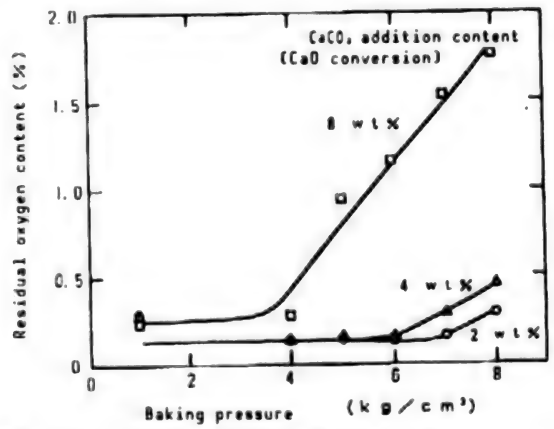

Figure 2. Relationship Between Residual Oxygen Content and Baking Pressure in Sintered Material

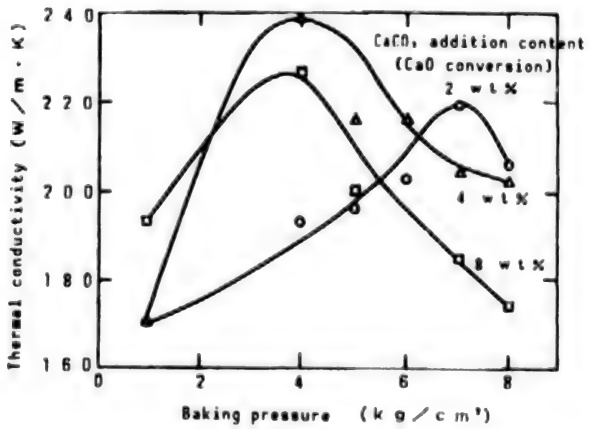

Figure 3. Relationship Between Thermal Conductivity and Baking Pressure

By using micro section X-ray diffraction to analyze a sample that had been baked at a higher pressure than this baking pressure, calcium aluminates $CaO \cdot 6Al_2O_3 (CA_6)$ and $3CaO \cdot Al_2O_3 (C_3A)$ were identified in addition to the AlN

crystals. This indicates that the calcium aluminates generated were not of a single composition, but were composed of two types of substances with different compositions. In addition, since the residual calcium and oxygen contents in the sintered material do not remain in proportion to the added $CaCO_3$ content, it can be considered that the composition of calcium aluminates generated differs according to the added content of $CaCO_3$. Therefore, it is believed that the maximum value of thermal conductivity shifts to the low baking pressure side when the added amount of $CaCO_3$ is great.

3.3 SEM Observation

Figure 4(a) [not reproduced] shows the rupture surface of a sintered material with an added $CaCO_3$ content of 2 wt percent and baked at a pressure of 7 kg/cm^2, while Figure 4(b) [not reproduced] shows the rupture surface of a sintered material with an added $CaCO_3$ content of 2 wt percent and baked at a pressure of 1 kg/cm^2 (atmospheric). There are no inclusions among the crystal grains and particles have grown in Figure4(a) [not reproduced]. However, the crystals assume a roundness and inclusions exist among the particles in Figure 4(b) [not reproduced]. However, the crystals assume a roundness and inclusions exist among the particles in Figure 4(b) [not reproduced]. This demonstrates that the evaporation of the liquid phase differs according to the difference in baking pressure.

4. Conclusion

$CaCO_3$ was added as the sintering assistant, a liquid phase of calcium aluminate ($Ca_xAl_yO_z$) was generated, the effect of the baking pressure on liquid phase evaporation was studied in order to promote the thermal conductivity of AlN, and the following matters have been made clear.

(1) Calcium aluminate generates crystals of different compositions such as $CA_6(CaO \cdot 6Al_2O_3)$ and $C_3A(3CaO \cdot Al_2O_3)$, according to the added $CaCO_3$ content.

(2) Since the composition ratio of calcium aluminate differs, the vapor pressure differs according to the baking pressure.

(3) Therefore, the baking pressure under which the thermal conductivity reaches a maximum differs according to the added $CaCO_3$ content and, the greater the $CaCO_3$ content, the more the baking pressure shifts to the low pressure side. When $CaCO_3$ is added at 4 wt percent by CaO conversion and a baking pressure of 4 kg/cm^2 has been utilized, thermal conductivity becomes maximal at 240 $W/m \cdot k$.

References

1. Electronic Material Editorial Department, ed., "Hybrid Mounting Technology," Industrial Research Association, 1988, pp 106–117.

2. Kuramoto, N. and Taniguchi, H., J. MAT. SCI. LETT., Vol 3, 1984, pp 471–474.

3. Sakai, T., Kuriyama, M., Inukai, T. and Kijima, T., CERAMICS INDUSTRY ASSOCIATION MAGAZINE, Vol 86, 1978, p 30.

4. Horiguchi, A., Kasori, M., Ueno, F. and Takushoku, Ak., "1985 Ceramics Association Annual Meeting Manuscripts," 1989, p 969.

5. Kurokawa, Y., Hamaguchi, H., Shimada, Y., Utsumi, K. and Takamizawa, H., "Proc. of 1987 ISHM," 1987, p 654.

Thick Film Resistor for Use in AlN Ceramics

43067199E Tokyo MES'89 in Japanese 17-18 Jul 89 pp 133-136

[Article by Yasutoshi Kurihara, et al., Hitachi, Ltd.]

[Text] The resistance value and TCR control and reliability confirmation were promoted for the purpose of developing a RuO_2 system thick film resistor for AlN ceramics. As a result, a resistor of several dozen Ω/aperture to several dozen kΩ/aperture was obtained by combining crystallized glass with a PbO content of about 6 wt percent (thermal expansion coefficient: 3.6 x 10^{-6}, softening point 610°C) with RuO_2. The resistor of the above system to which metallic oxide had been added indicated a TCR ±250 ppm/°C (30 Ω/aperture~ 30 kΩ/aperture), and the resistance value variation following the heat cycle test (-55~150°C, 1000 times) and high temperature shelf test (150°C, 1000 hr) was less than +1 percent, demonstrating superior stability. In addition, studies were made of the effect of the particle diameter on electrical characteristics.

1. Introduction

AlN ceramics possess production advantages such as enabling green sheeting and atmospheric sintering to be conducted,[1-3] in addition to having physical properties suitable for semiconductor mounting.[1-5]

The hybrid IC mounted on a power semiconductor represents one of the prominent AlN application fields, and the development of a thick film material necessary in this regard is also being promoted. Nevertheless, its practical application has not progressed much. The fact that a resistor capable of practical application has not yet been developed can be listed as one of the reasons for this. In other words, it is basically necessary that it excel in 1) resistance value controllability and 2) controllability of TCR and stability against thermal stress, however, the current status remains as that mentioned above.

On the other hand, it is desirable from the circuit design standpoint that the resistor cover a wide ranging resistance area. However, problems exist, such as the resistance paste containing PbO system glass, which is often used for alumina, being difficult to use for AlN,[9,11] and it cannot entirely satisfy this demand.

Therefore, a resistor of less than 10 kΩ/aperture with a comparatively high demand was trial manufactured for the purpose of developing an AlN thick film resistor with potential for practical use, and the resistance value and TCR control and reliability confirmation have been promoted in this research.

2. Experimental Method

2.1 Preparation of Resistance Paste and Sample

The AlN substrate used in this research was a high purity sintered material (25.4 x 25.4 x 0.63 mm) with a density of 3.3 g/cm^3, thermal conductivity of 140 W/m·K (RT), thermal expansion coefficient of 4.4 x 10^{-6}/°C and volume resistivity of 10^{14}Ω·cm (RT). In addition, a 96 percent alumina substrate was also used for the standard sample.

The resistor paste was obtained by kneading the conductive particles, binder and organic vehicle by using a triple roll. A metallic oxide powder for TCR adjustment was added to this when necessary. Two types of RuO_2 powders with different particle diameters (RuO_2A:3.5~15 μm, RuO_2B: 0.3~1.6 μm) were used for the conductive particles. Table 1 shows the physical properties and components of the glass powder. The glass was selected by taking into consideration the low expansion coefficient, high softening point and small PbO content point. The [conductive particle (RuO_2)/binder (glass)] mixing ratio will be shown hereafter by the weight ratio.

Table 1. Physical Properties and Composition of Glass

Physical properties	TEC* (10^{-6}/°C)	Softening point (°C)	Density (g/cm^3)
	3.6	610	3.9
Constituents	SiO_2–B_2O_3–PbO–ZnO		
PbO content	5.9 wt%		

*Thermal expansion coefficient

Figure 1 shows the evaluation sample. This sample was prepared according to the following procedure. First of all, the Ag·Pd paste was printed on the substrate and, after leveling at room temperature and a drying treatment of 150°C x 3 minutes, the conductor was formed by baking in air at 850°C x 10 minutes. Then, after going through, in order, the printing and baking of the resistance paste and printing and baking (600°C x 10 minutes) of the overcoat paste by a similar process, the resistor and overcoat layer were formed. The thickness of each layer was 12±1 μm.

2.2 Evaluation and Reliability Test of Resistor

The resistance value between A–A′ of Figure 1 was measured and converted into the sheet resistance. TCR showed a value between room temperature and 125°C,

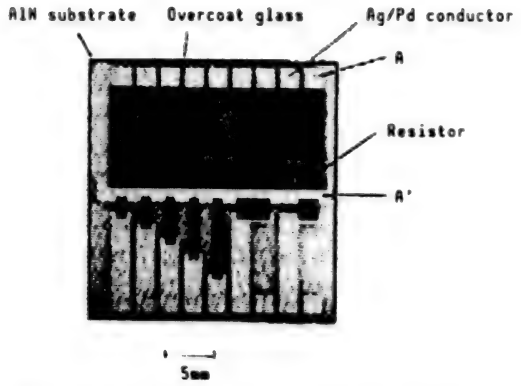

Figure 1. Sample for Evaluation

but this target value was made ±250 ppm/°C. The resistance value stability was evaluated by tracking the sheet resistance under the heat cycle test (-55~150°C, 1000 times) and high temperature shelf test (150°C, 1000 hours). The stability guidelines were reached when the resistance value variation was within ±1 percent of the initial value. Analyses of the resistor, etc., were also attempted.

3. Experimental Results and Studies

3.1 Reaction of Glass and AlN

According to a previous report,[9] the higher the PbO content and the lower the softening point of a glass, the more conspicuous is the reaction with AlN, and foaming and conductive particle condensation are generated. The glass used in this research contains a small amount of PbO, as shown in Table 1 and, based on the phenomenon mentioned above, an adverse effect on the resistance value is feared. For this reason, it is important that the resistor be firmly joined to the substrate, and it is necessary that the glass have a suitable reactivity and wetness with AlN. Therefore, the affinity between the glass material and AlN is checked first.

Table 2 shows the NO_x gas generation content through heat treatment (850°C x 10 minutes) in an oxygen ventilating current of the substrate printing the resistance paste (mixing ratio: 20:80). The NO_x gas content in this case was obtained by using ion chromatography to analyze the alkali solution collecting the generated gas. Paste No 1 has a small content of PbO and uses a high softening point glass, however, the NO_x content is small and the same in both the AlN and alumina, and a significance difference between the two could not be found. On the other hand, paste No 2, having a high PbO content and using a low softening point glass, has a small amount of NO_x generated for alumina, while the NO_x generation is extremely great in the AlN combination. For the reasons mentioned above, it is judged that adding the glass powder to paste No 1 has the potential for being applicable as a resistor since it does not generate an excessive reaction with AlN.

Table 2. Relationship Between Type of Glass and NO_x Gas Generation Volume

Paste No.	Physical properties of glass			NO_x gas generation volume (μl/g)	
	PbO content	Softening point	Remarks	AlN substrate	Alumina substrate
1	5.9 wt%	610°C	See Table 1	0.04	0.03
2	82.0 wt%	382°C	*	0.35	0.06

*: Composition (wt%) $TiO_2(9)$-$B_2O_3(8)$-PbO(82)

3.2 Mixing Ratio of RuO_2 and Glass

The electrical characteristics of thick film resistors are basically determined by the mixing ratio of RuO_2 and glass.[13] However, they are also delicately affected by the physical properties and particle diameter of the powders. Therefore, the controllability of the resistance value and TCR for basic combination consisting of RuO_2A and glass A has been confirmed. The relationship between the mixing ratio and resistance value is shown in Figure 2. The resistance value changes from about 10 kΩ/aperture at the mixing ratio of 40:60 to about 10 Ω/aperture at the mixing ratio of 70:30. The objective resistance value range can be controlled by means of the combination mentioned above.

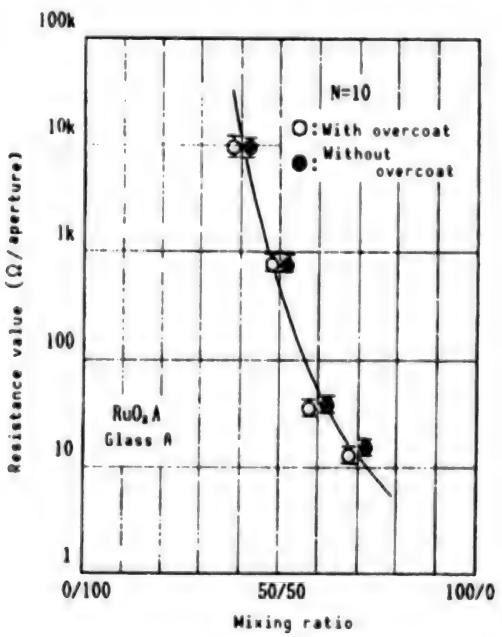

Figure 2. Relationship Between Mixing Ratio and Resistance Value

Figure 2 shows the relationship between the resistance value and TCR for the combination mentioned above. TCR adopts a large positive value in the low resistance area and gradually shows a small positive value as it moves toward the high resistance area. A value of less than +250 ppm/°C is shown in the range exceeding 1 kΩ/aperture, and the targeted TCR value is available without additions or special improvements. However, TCR is too high in the low resistance area and its improvement is necessary.

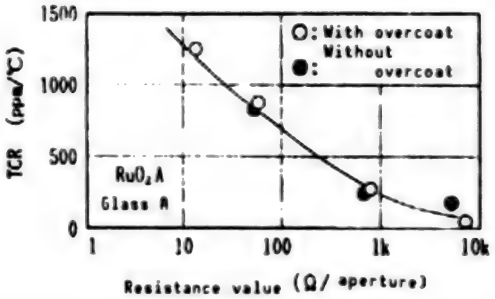

Figure 3. Relationship Between Resistance Value and TCR

3.3 Effect of Powder Grain Size on Electrical Characteristics

Figure 4 shows the effect of powder grain size on the resistance value. Curve I shows this effect for the RuO_2B and glass A combination, curve II for the RuO_2A and glass B combination and curve III shows it for the basic combination mentioned above. Curve I, when compared to curve III, has shifted to the low resistance side, but the mixing ratio dependency of the resistance value is particularly small in the area of less than 100 Ω/aperture. This means that the resistance value of the low resistance area can be controlled well. It was pointed out in the previous report that the contact probability increases when the conductive particles become finer, facilitating the formation of a conductive network.[3] It is believed that the trend of curve I in this research is based on the same reason. On the other hand, curve II, when compared to curve III, has shifted to the high resistance side. This trend is caused by the decreasing density of RuO_2 intervening in the glass intergranular when glass particles become fine, and the contact probability among RuO_2 particles drops.[13] The degree of shifting to the high resistance side remains within narrow limits. This is because the glass particle size is 19 μm for curve II and 3.3 μm for curve III, and the size difference is small.

Figure 5 shows the effect of powder particle size on TCR when compared with the results (curve III) of Figure 3. Curve I shows this effect for the RuO_2B and glass A combination, while curve II shows it for the RuO_2A and glass B combination. Both curves I and II have shifted to the low TCR side in comparison to curve III. The shifting degree is greater in curve I than in curve II and, moreover, it is conspicuous on the low resistance side. These results show that the fining of the conductive particle or binder is effective for low TCR-izing.

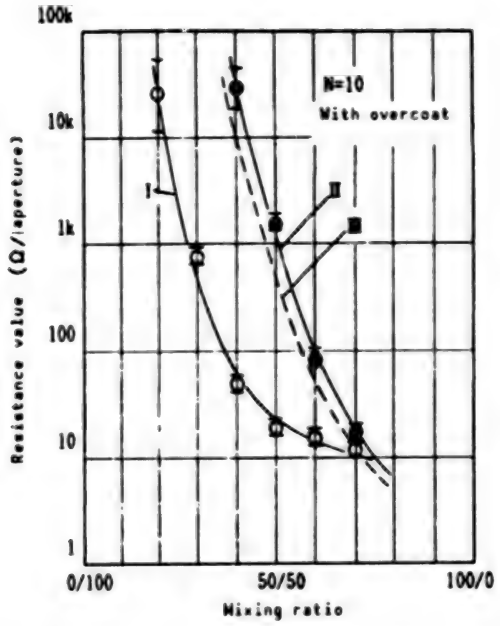

Figure 4. Effect of Powder Particle Diameter on Resistance Value

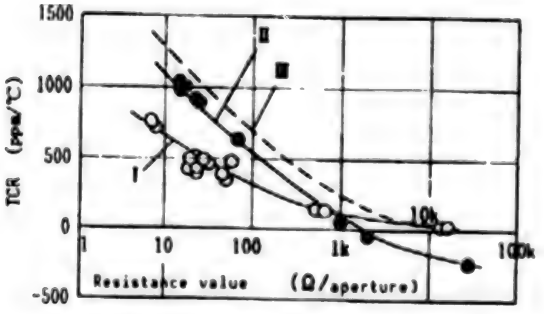

Figure 5. Effect of Powder Particle Diameter on TCR

It is thought that when the RuO_2 addition is great, the conductive path of the resistor consists of 1) a conductive chain by sintering or RuO_2 particle contact, or 2) conductive chain through the medium of an extremely thin glass layer (layer doped with RuO_2). Therefore, electrical conductivity by (1) above is dominant in a small resistance value area, and since it can be affected by RuO_2 with a large value of +4950 ppm/°C, it is believed that the TCR will indicate a large positive value. As the addition content to RuO_2 decreases, it will be subject to the influence of (2) above, i.e., the influence of a small tunnel conductance,[14] and the TCR will drop. In addition, case 3) will develop in which a conductive chain is formed through the thick glass layer when RuO_2 decreases further and the contact probability is reduced and, since hopping conductance (semiconductive and TCR is negative) by way of the impurity level is dominant, it is believed that the TCR will continue to approach the negative side.

Curve II, when compared to curve III, has a smaller glass particle size, the contact probability f conductive particles is reduced,[13] and the mechanism of (2) and (3) above is susceptible to electric conduction. As a result, it can be thought that the TCR has shifted more to the negative side than that of curve III over the entire resistance area. Meanwhile, the characteristic points in curve I are that low TCR-izing is remarkable in the low resistance area and a negative value is not shown at more than 1 kΩ/aperture. Spacing among the conductive particles is reduced when RuO_2 is comprised of fine particles. When mechanism (1) is dominant due to RuO_2 contact, however, a TCR reduction on the low resistance side will hardly be possible. In addition, when conductance in more than 1 kΩ/aperture is controlled by mechanism (3), curve I, similarly to curve II, should show a negative value, but the value obtained is positive. When taking these points into consideration, it can be presumed that curve I is strongly affected by mechanism (2) above, i.e., tunnel conductance.

3.4 TCR Adjustment by Additives

The smallest value shown in Figure 5 for the curve I combination occurred when the resistor was composed solely of RuO_2 and glass. Since the range that satisfies the targeted TCR value (±250 ppm/°C) is more than 200 Ω/aperture, further low TCR-izing of the low resistance area is necessary. Therefore, the addition of a TCR adjusting agent was attempted in the curve I system mentioned above.

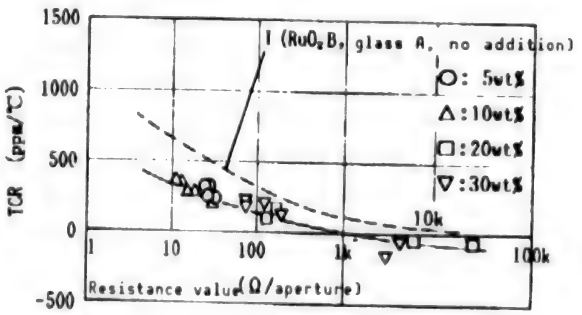

Figure 6. Relationship Between Resistance Value and TCR When Adding Metallic Oxide

Figure 6 shows the relationship between the resistance value and TCR when metallic oxide has been added, and a comparison with the system having no additions is shown. The TCR of the metallic oxide-added system shifted further toward the negative side than did the system with no additions over the entire resistance area checked, and the effect of low TCR-izing by the oxide addition is recognized. In addition, the targeted value was satisfied at resistance values of more than 30 Ω/aperture. The oxide addition has been attempted in the range of 5~30 wt percent, but the effect obtained by increasing the addition content is not as conspicuous. Similar studies were also promoted for combinations of curves II and III in Figure 5, but conspicuous effects of low TCR-izing were not recognized, nor were they when increasing the oxide addition content. Therefore, it is believed that studies

on various additives[15] are necessary in order to promote further low TCR-izing of the low resistance area.

3.5 Stability of Resistance Value

Although the resistor is subjected to various thermal stresses under actual operation conditions, it must also demonstrate a stabilized resistance value under such conditions. Figure 7 shows the fluctuation of the resistance value according to the heat cycle and high temperature shelf tests. It can be recognized from Figure 7 that 1) fluctuation is great in the low resistance area when an overcoat is not provided, and 2) the resistor has superior stability over the entire resistance area (especially in the low resistance area) and the targeted value (±1 percent) is satisfied when an overcoat is provided.

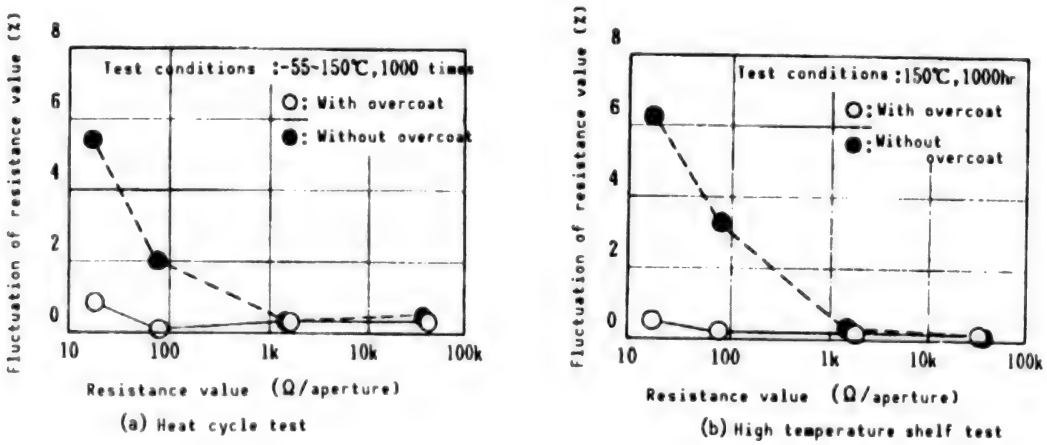

Figure 7. Stability of Resistance Value

It is believed that trend (1) is attributable to the following reason. The more the RuO_2 content is increased, the greater is the thermal expansion coefficient of the resistor as a complex. As a result, a tensile stress acts on the resistor on the AlN substrate, disconnection of the conductive network progresses, and the resistance value increases. However, in many cases the glass content has a small thermal expansion coefficient in the range exceeding 1 kΩ/aperture, the tensile stress does not have much of an effect, network disconnection is controlled and the resistance value stabilizes. Trend (2) is due to the tensile stress working on the resistor being compensated for by the overcoat glass with a low thermal expansion coefficient and disconnection of the conductive network being controlled. The overcoat glass, as seen here, not only protects the resistor surface mechanically and chemically in an AlN substrate with a small thermal expansion coefficient, but is also extremely important for stabilizing the resistance value by means of stress compensation.

4. Conclusion

The resistance value and TCR control and resistor reliability were promoted for the purpose of developing a RuO_2 thick film resistor for AlN ceramics, and the following conclusions were obtained.

(1) A resistor of from several dozen Ω/aperture to several dozen kΩ/aperture was available by combining crystallized glass with a PbO content of about 6 wt percent (thermal expansion coefficient: 3.6×10^{-6}/°C, softening point: 610°C) and RuO_2.

(2) A resistor in which metallic oxide had been added to the system mentioned above indicated TCR ±250 ppm/°C (35 Ω/aperture~30 kΩ/aperture) and the resistance value variation after the heat cycle (-55~150°C, 1000 times) test and high temperature (150°C, 1000 hr) test was less than 1 percent.

(3) The resistance value shifted toward the low resistance side when the RuO_2 particle diameter was small and toward the high resistance side when the RuO_2 particle diameter was large. TCR shifts toward the negative side when the glass or RuO_2 particle diameter is small.

References

1. Kuramoto, N. and Taniguchi, H., J. MATERIALS SCIENCE LETTERS, Vol 3, 1984, pp 471-474.

2. Kuramoto, N., et al., IEEE TRANS., C.H.M.T., Vol CHMT-9 No 4, 1986, pp 386-390.

3. Iwase, N., et al., Ibid., Vol CHMT-8 No 2, 1985, pp 253-258.

4. Kurokawa, Y., et al., Ibid., pp 247-252.

5. Werdecker, W., "Proc. Fifth European Hybrid Microelectronics Conf.," 1985, pp 472-488.

6. Mohammed, A.A. and Corbett, S.J., "Proc. 1985 International Symposium on Microelectronics," 1985, pp 218-224.

7. Detter, E.S. and Charles, Jr., H.K., "Proc. 1987 International Symposium on Microelectronics," 1987, pp 19-29.

8. Soji, et al., "Manuscripts for Second Microelectronics Symposium," 1987, pp 209-212.

9. Kubota, et al., "Proc. Fifth International Microelectronics Conf.," 1988, pp 137-141.

10. Yoneda, Y., et al., Ibid., pp 147-152.

11. Allison, K., et al., "Thick Film Materials for Applications on Aluminum Nitride Substrates: Proc. Fifth International Microelectronics Conf.," 1988, pp 153-160.

12. Cox, V., INTERNATIONAL J. HYBRID MICROELECTRONICS, Vol 10 No 3, 1987, pp 8-12.

13. Inokuma, T., et al., IEEE TRANS., C.H.M.T., Vol CHMT-7 No 2, 1984, pp 166-175.

14. Ito, et al., "Manuscripts for Second Microelectronics Symposium," 1987, pp 201-204.

15. Inokuma, T. and Taketa, Y., ACTIVE AND PASSIVE ELEC. COMP., Vol 12, 1987, pp 155-166.

Y-Ba-Cu-O Superconducting Thin Film Formation, Effect of Buffer Layer

43067199F Tokyo MES'89 in Japanese 17-18 Jul 89 pp 180-183

[Article by Kan Kubota, et al., Shinshu University]

[Text] A $YBa_2Cu_3O_{7-x}$ (Y-Ba-Cu-O) superconducting thin film was formed on a single crystal Si (100) substrate by the DC magnetron sputter method. A resistance transition was observed at 92 K, and the potential for realizing a superconducting thin film on a Si substrate was recognized. An evaluation was made of the basic characteristics of thin films, and studies were conducted on the effect of the YSZ (yttria-stabilized-zirconia) buffer layer used to prevent counter diffusion.

1. Introduction

Reports have been made in recent years on the discovery of oxide superconductors. These oxide superconductors include those of the Y system[2-4] which currently exceed the critical temperature of 92 K, Bi system,[5] etc., as well as those of the Ba system.[1] Of these, the Y system oxide superconducting material has attracted attention as the first high temperature superconducting material that is usable in a liquid nitrogen atmosphere, and it currently serves as the basic material used in discussing various superconducting characteristics, processing technologies, applications to electronic devices, etc.[6]

The following are problems involved in the thin filming of these superconductors:

(1) Realization of stoichiometric composition ratio (Y:Ba:Cu=1:2:3).

(2) Control of oxygen concentration in crystal.

(3) Prevention of counter diffusion between substrate material and thin film.

In the Y system, superconductivity is not exhibited in any phases other than $YBa_2Cu_3O_{7-x}$. Therefore, a strict composition ratio of Y, Ba and Cu is demanded in the film.[6] As for controlling the oxygen temperature, since it has been reported that a high critical temperature is available when the value of x is 0-0.2 in the superconductor composition formula $YBa_2Cu_3O_{7-x}$,[7] the introduction

of oxygen into the thin film is indispensable. In addition, since the deviation of the stoichiometric composition ratio due to the counter diffusion between the substrate material and thin film, as well as the formation of a nonsuperconducting phase in the film by this deviation, can pose problems, the usable substrate is limited, and thin filming on single crystal insulating substrates ($SrTiO_3$, MgO) is the main current now.[8-11] However, these substrates are high in cost, and this fact can represent an obstacle when realizing a cost down of thin filming devices.

Therefore, we formed a Y-Ba-Cu-O superconducting thin film on a Si substrate by the DC magnetron sputter method in an attempt to realize a superconducting thin film on other types of substrates and with the intention of applying to high-speed superconductor devices.[11-14] The crystallinity and electrical characteristics of the formed thin films were evaluated. In addition, a YSZ (yttria-stabilized-zirconia) buffer layer was formed to prevent counter diffusion, and the effect was studied.

2. Formation of Y-Ba-Cu-O Thin Film

In this research, a YSZ buffer layer was formed on a substrate by the RF magnetron sputter method, and a Y-Ba-Cu-O thin film was then formed on top of this buffer layer. YSZ formation was conducted under a high-frequency electric power of 70 W and a substrate temperature of 700°C by using a ZrO_2 (Y_2O_3:8.3 mol percent addition) sintered material target.[13] A DC magnetron sputter device was used and a Y-Ba-Cu-O thin film was formed, with the sintered material as the target. Figure 1 shows the schematic diagram of the DC magnetron sputter device. The sputtering target used was pressure formed by mixing Y_2O_3, $BaCO_3$ and CuO powders and sintering them for 2 hours at 900°C, and the composition ratio was made Y:Ba:Cu=1:5:7 and 1:5.5:6.5 (mole ratio) by taking into account the film composition upon film formation.

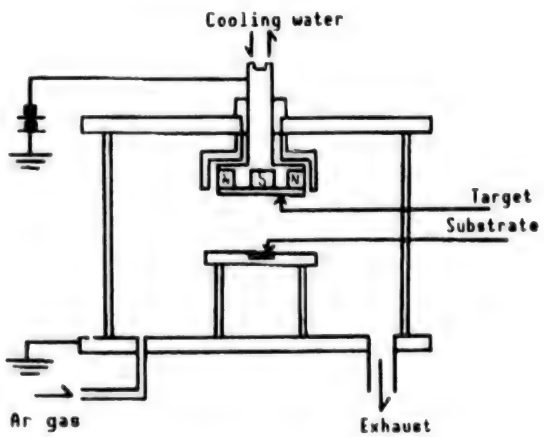

Figure 1. Schematic Diagram of DC Magnetron Sputter Device

Typical film formation conditions are shown in Table 1. Thin film forming was conducted by flowing in Ar gas after exhausting the reaction chamber interior to less than 1 x 10^{-3} Torr, fixing the pressure at reaction to 30 x 10^{-3} Torr

and applying DC voltage to the electrode. The input electric power was fixed at 30 W. Substrate heating was not conducted during thin film formation, and the crystallization of thin film and introduction of oxygen into the crystal were made by heat treating after forming.

Table 1. Y-Ba-Cu-O Thin Film Forming Conditions

Input electric power	30	W
Substrate temperature	Ambient	
Reaction indoor pressure	30×10^{-3}	Torr
Forming time	180~300	Minutes
Substrate	Single crystal Si (100)	
Film thickness	1~1.5	μm
Target composition ratio	Y:Ba:Cu-1:5:7,1:5.5:6.5	
Heat treatment temperature, time	Crystallization: 750~900 15~180 Oxidation: 400~600 60	°C Minutes °C Minutes
Oxygen flow rate	0.2~0.9	ℓ/min
Buffer layer	YSZ: 0.2, 0.6	μm

3. Results and Discussion

3.1 Evaluation of Y-Ba-Cu-O Thin Film Crystallinity

Figure 2 shows the X-ray diffraction results of the Y-Ba-Cu-O thin film with changes in the heat treatment temperature 1) when not using a buffer layer and 2) when using a buffer layer. The heat treatment lasted 15 minutes and the oxygen flow rate was fixed at 0.2 ℓ/min in both cases. The diffraction pattern from the Si (100) single crystal surface used for the substrate and from the YSZ used as the buffer layer has been omitted, while the diffraction angle ranging from 20~80° is shown.

A diffraction peak exhibiting a superconducting phase could not be observed in the sample lacking a buffer layer under any heat treatment temperatures, and the formation of Ba_2 SiO_4 due to the counter diffusion of the film and substrate was recognized. In contrast to this, diffraction by the dominant orientation surfaces (110) and (103) indicating the presence of a superconducting phase was observed in the sample using the buffer layer with heat treatment at 800°C, and this diffraction became stronger as the heat treatment temperature rose to 850°C. However, the diffraction peak indicating a superconducting phase disappeared at heat treatment of 900°C, and a diffraction peak, although slight, of a compound formed by the reaction of the film and

substrate was observed. It was ascertained from these results that it was possible to form a Y-Ba-Cu-O thin layer on the Si substrate by using a buffer layer. In addition, it is believed that the optimum heat treatment temperature is around 850°C when the crystallinity and counter diffusion of the film are taken into consideration.

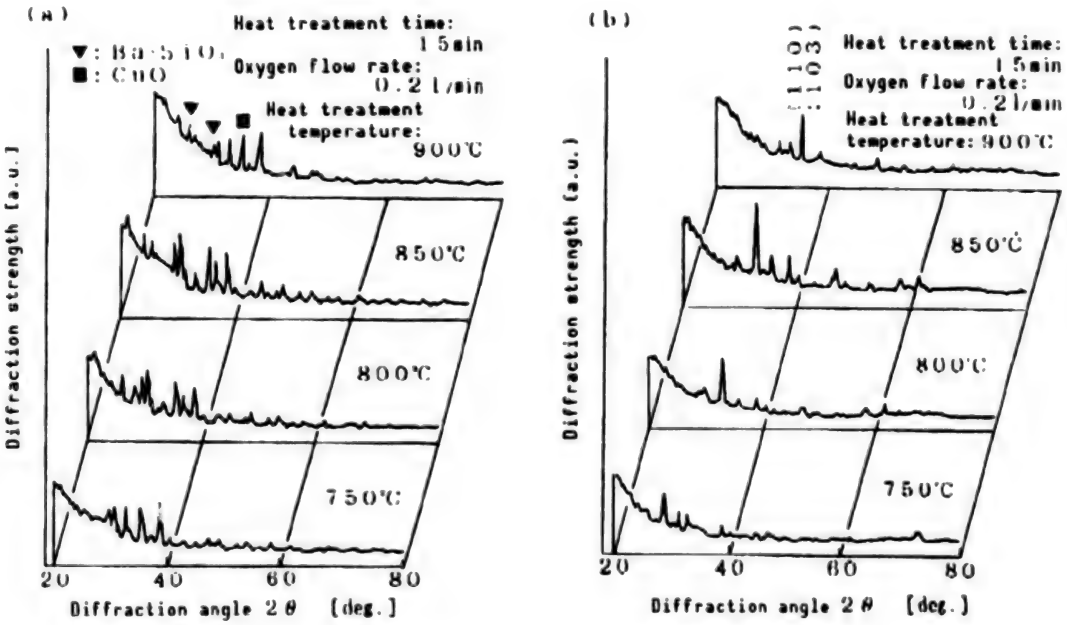

Figure 2. Heat Treatment Temperature Dependence of X-Ray Diffraction Pattern
(a) When not using a buffer layer
(b) When using a buffer layer

3.2 Evaluation of Electrical Characteristics of Y-Ba-Cu-O Film

As ascertained from the X-ray diffraction results, the formation of a superconducting phase was recognized and superconductivity was not available in the sample in which a buffer layer was not used. In contrast to these results, although an offset temperature was not available, a resistance transition state (onset temperature) was observed when a buffer layer was utilized. The specific resistance-temperature characteristics when changing the heat treatment time at the temperature of 850°C (considered to be the optimum temperature) are shown in Figure 3. The value of an onset of 56 K has been obtained by this in the heat treatment time of 60 minutes.

In addition, the specific resistance-temperature characteristics when increasing the oxygen flow rate from 0.21 ℓ/min to 0.91 ℓ/min and the conducting heat treatment so that oxygen of a higher concentration can be introduced into the film crystals is shown in Figure 4. The specific resistance of the film became about 1 digit smaller, the onset temperature was raised to 92 K, and an improvement in the film characteristics was seen by conducting heat treatment in oxygen at a higher concentration.

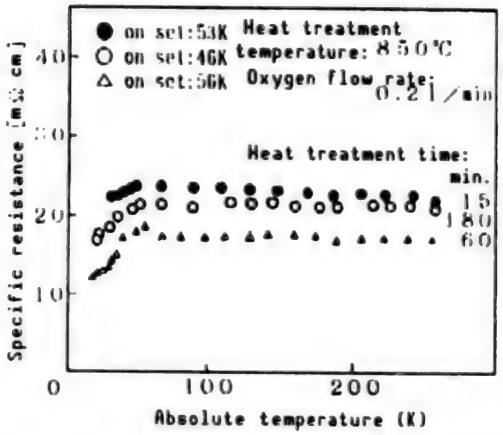

Figure 3. Specific Resistance–Temperature Characteristics

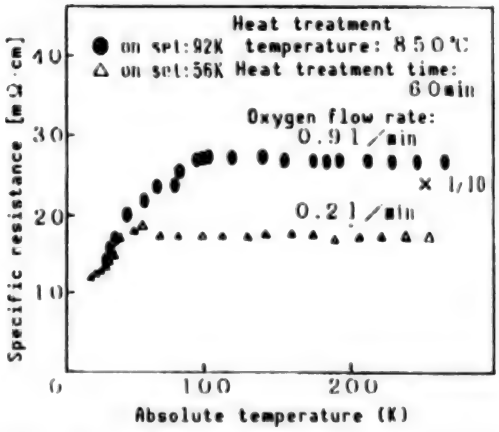

Figure 4. Specific Resistance–Temperature Characteristics

From the results mentioned above, it can be recognized that the use of a buffer layer is indispensable when forming a Y–Ba–Cu–O thin film on an Si substrate. However, an offset temperature has not been obtained in this research, and it is believed necessary to study the stricter composition control of the film and a process for introducing a higher oxygen concentration into the film in order to realize this improvement.

3.3 Effect of Buffer Layer

It was ascertained from the X-ray diffraction measurement results and electrical characteristics that the diffusion of the Si substrate material into the film exerts a great effect on the film characteristics. Therefore, the status of Si diffusion into the film when changing the heat treatment temperature has been observed by the electron probe microanalysis (EPMA) method, and the results are shown in Table 2. The film thickness of the buffer layer was changed at 850°C. The diffusion of Si into the film is practically not seen up to the heat treatment temperature of 850°C, when the film thickness of the buffer layer is about 0.2 μm. Since diffusion starts at 900°C, however, it is believed that Si diffusion cannot be prevented at high

temperatures, even when using a buffer layer. The Si diffusion value becomes less than the measuring limit when the film thickness of the buffer layer is from 0.2 μm to 0.6 μm at a heat treatment temperature of 850°C, and it is believed that diffusion into the film can be prevented. Figure 5 shows the thin film constituent elements and the diffusion state of the substrate material when the film thickness of the buffer layer is 0.6 μm. Since Si diffusion into the film is not observed when the film thickness of the Y-Ba-Cu-O thin film is about 1.2 μm, nor is the diffusion of thin film constituent elements to the substrate, the effect of the YSZ buffer layer in preventing counter diffusion is recognized as being significant.

Table 2. Si Dispersion Into Thin Film

(Analysis area: ~1.2 μm)

Heat treatment temperature (YSZ film thickness)	Dispersion content of Si (c.p.s.)	
	With buffer layer	Without buffer layer
800°C (0.2 μm)	Nil (2)	Possessed (40)
850°C (0.2, 0.6 μm)	Nil (3.0)	Possessed (40)
900°C (0.2 μm)	Possessed (12.5)	Possessed (50)

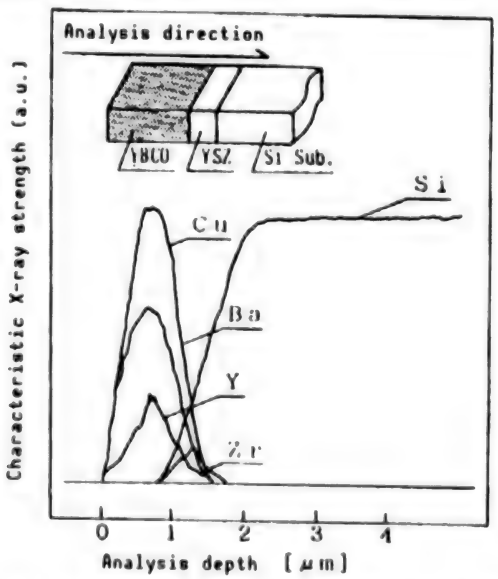

Figure 5. Analysis of Fracture Surface of Y-Ba-Cu-O Thin Film

4. Conclusion

In this research, the basic characteristics of thin films obtained by the DC magnetron sputter method for the purpose of forming a Y-Ba-Cu-O thin film on an Si substrate have been evaluated, and studies on the YSZ buffer layer effect conducted, resulting in the following findings:

(1) A polycrystal Y-Ba-Cu-O thin film was obtained only when the buffer layer was used at a heat treatment temperature exceeding 800°C.

(2) A thin film exhibiting an onset temperature of 92 K was obtained by conducting heat treatment at 850°C for 60 minutes and increasing the oxygen flow rate during the heat treatment.

(3) It was recognized that the YSZ buffer layer prevents counter diffusion between the film and substrate up to a heat treatment temperature of 850°C.

Although it was not possible in this report to form a thin film showing an offset temperature in the superconducting range, it was confirmed that the separation of the film and substrate was possible by using the YSZ buffer layer. We believe that it will be possible in the future to form thin films exhibiting superior characteristics strictly controlling the film composition and oxygen introduction into crystals during the heat treatment process.

References

1. Bedonorz, J.B. and Muller, K.A., Z. PHYS., Vol B64, 1986, p 189.

2. Wu, M.K., Ashburn, J.R., Torng, C.J., Hor, P.H., Meng, R.L., Gao, L., Huang, Z.J., Wang, Y.Q. and Chu, C.W., PHYS. REV. LETT., Vol 58, 1987, p 908.

3. Oda, Y., Nakada, I., Kohara, T. and Asayama, K., J.J.A.P., Vol 26, 1987, p L608.

4. Takayama-Muromachi, E., Uchida, Y., Matsui, Y. and Kato, K., Ibid., p L619.

5. Maeda, H., Tanaka, Y., Fukutomi, M. and Asano, T., Ibid., Vol 27, 1988, p L209.

6. Kono, et al., SENSOR TECHNOLOGY, Vol 9, 1989, p 54.

7. Izumi, et al., ELECTRONICS•CERAMICS, 1988, p 18.

8. Sorimachi, Y., Kobayashi, A., Yamashita, T., Takata, M., Miyauchi, S. and Tsubata, I., J.J.A.P., Vol 26, 1987, p L1451.

9. Ohkuma, H., Mochiku, T., Kanke, Y., Wen, Z., Yokoyama, S., Asano, H., Iguchi, I. and Yamaka, E., Ibid., p L1484.

10. Aida, T., Fukuzawa, T., Takagi, K. and Miyauchi, K., Ibid., p L1489.

11. Terada, Ihara and Hirabayashi, "Research Report of Electronic Information Communication Society," CPM87-4, 1987, p 19.

12. Onuma, Y., Kamimura, K., Nakao, M., Kunugi, K. and Kubota, M., J.J.A.P., Vol 27, July 1988, pp 1351-1352.

13. Konuma, Sotomura, Yamakawa, Nakao and Kamimura, THESIS MAGAZINE A, Japan Electric Society (Scheduled for publication in July edition).

Atomic Layer Epitaxy of ZnSe

43067199G Tokyo MES'89 in Japanese 17-18 Jul 89 pp 184-187

[Article by Tamotsu Okamoto, et al., Chiba University]

[Text] Since the atomic layer epitaxy (ALE) method conducts atom growth by layers, it is a crystal growth method that is capable of controlling film thickness by atomic layer accuracy and has the potential of obtaining high quality crystals. The potential for ALE growth of ZnSe, that is anticipated to serve as a blue luminescent device material, was studied by the metallo-organic molecular beam epitaxy (MOMBE) method in this research, and a study of the growth mechanism and evaluation of the film quality were conducted.

1. Introduction

ZnSe is a compound semiconductor anticipated to serve as a blue luminescent device material. However, since the growth temperature of this crystal is high under the conventional crystal growth method, the so-called self-guarantee effect exerts a strong influence, control of physical properties is difficult, and the development of a new crystal growth method is necessary in order to solve this problem. The atomic layer epitaxy (ALE) method involves growing atoms by layers by supplying materials one after another. This method not only allows the film thickness to be strictly controlled by atomic layer accuracy during the compound semiconductor growth, but there is also the possibility of obtaining extremely high quality crystals with minor defects. Therefore, the preparation of a high quality ZnSe thin film can be expected by applying the ALE method to ZnSe growth. ALE growth was originally realized in the growth of ZnS film, employing $ZnCl_2$ and H_2S as materials.[1] Studies have been actively conducted since then in the range of III-V group compounds, such as GaAs, etc., and thin films of good quality have been obtained.[2-4] However, reports on the ALE growth of ZnSe have only referred to those employing the MBE method up to now,[5-7] and great interest is being shown in whether the ALE growth of ZnSe, utilizing the chemical reactions of materials such as in the MOCVD method, will be possible. Therefore, in this research the ALE growth of ZnSe was studied by the MOMBE method, using DMZn and H_2Se as materials.

The MOMBE method can supply Zn and Se to the substrate by conducting material gas cracking. Since not only the ordinary "MBE type" growth that supplies the simple substances of Zn and Se as molecular beams is realizable, but also the

DMZn and H_2Se materials do not associate in the gas phase and are supplied as they are on the substrate when cracking is not conducted, a "CVD type" growth by the chemical reaction of other material members can also be realized. Therefore, ALE growth was respectively attempted in this research for cases when material gas cracking was conducted and when it was not conducted. Together with specifically studying the growth mechanism of the "CVD type" ALE growth of ZnSe which had not been studied previously, the film quality was compared by photoluminescence, etc.

2. Experimental Method

The turbo-molecular pump was used as the main pump in the MOMBE device in this research, and material molecules arrived directly at the substrate without associating with other gas molecules when conducting growth in a vacuum at about 10^{-5} Torr. DMZn and H_2Se of 100 percent were used as materials, and thermal decomposition (cracking) was enabled before reaching the substrate by means of the cracking cell at the nozzle tip. It is believed that the DMZn and H_2Se material decompose when cracking is conducted, and they become Zn and Se molecules, respectively. However, the cracking cell temperature is about 860°C for DMZn and about 680°C for H_2Se, and the decomposition efficiency of the material is about 75 percent.[8] It is basically necessary to supply materials alternately during ALE growth, and the alternate supplying of materials was realized in this system by interlocking and opening/closing the air valve of the material supply line and upper shutter on the substrate by computer control. The typical experimental conditions used in this research are shown in Table 1. The semi-insulating property (100) GaAs was used in this substrate.

Table 1. Main Growth Conditions

Substrate temperature	150~400 °C
DMZn feed supplied	5~20 μmol/min
H_2Se feed supplied	15,30 μmol/min
Supply frequency	1000,2000 cycle
DMZn pulse time	3 seconds
H_2Se pulse time	3 seconds
Purge time	5 seconds

3. When Cracking Both Materials

First of all, cracking of the DMZn and H_2Se materials was conducted and ALE growth was studied. Figure 1 shows the substrate temperature dependence of the growth rate. It is clear from this diagram that an ALE growth that becomes a single molecular layer per cycle of material feed can be realized at the substrate temperature of 200~275°C. The material supplied in this case is

sufficient for about five layers when taking into consideration the simultaneous supply results. When the DMZn and H_2Se materials are cracked, it is believed that they decompose and become Zn and Se_2 molecules, respectively,[8] and it is also believed that the growth mechanism becomes the same as that of the MBE method, making simple substances of the Zn and Se materials. In other words, when Zn or Se forms a single atomic layer, ALE growth is realized by the so-called self-stopping mechanism in which adsorption above a single atomic layer does not occur due to the reevaporation of the material adsorbed on the surface.

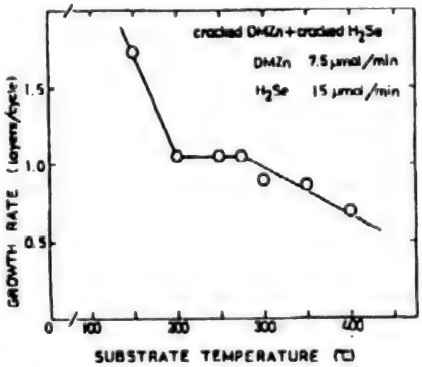

Figure 1. Substrate Temperature Dependence of Growth Rate

The growth rate increases at temperatures below 200°C, and it is thought that this increase occurs since excessive materials cannot reevaporate in the low temperature range. The growth rate decreases at temperatures exceeding 275°C, but it is difficult to say that the reason for this involves the reevaporation of the formed DMZn film. We have previously studied the Z film growth by simultaneously supplying DMZn and H_2Se in the MOMBE method and reported that a reduction in the growth rate occurred due to the drop of the material attachment coefficient at high temperatures.[8] It is believed that the reduction of the attachment coefficient at high temperatures will also occur in a similar manner when materials are supplied alternately, as in this research. Since the materials supplied decrease substantially when the attachment coefficient drops, ALE growth is not expected to be possible. The material supply content dependence of the growth rate at the substrate temperature of 300°C has been investigated to confirm this fact. Figure 2 shows the DMZn supply content dependence of the growth rate at a substrate temperature of 300°C. According to this diagram, ALE growth has been realized at a DMZn supply of 10 μmol/min, and it has been ascertained that the growth rate stopped at single layers for each cycle when the DMZn supply was increased. It can be said from this that reducing the attachment coefficient causes the growth rate reduction in the high temperature area. Therefore, there is a possibility that ALE growth can be realized by increasing the materials supplied in the high temperature area as well. In addition, an increase in the growth rate is not observed when increasing the materials supplied by the so-called self-stopping mechanism, and it can be confirmed that growth rate has occurred.

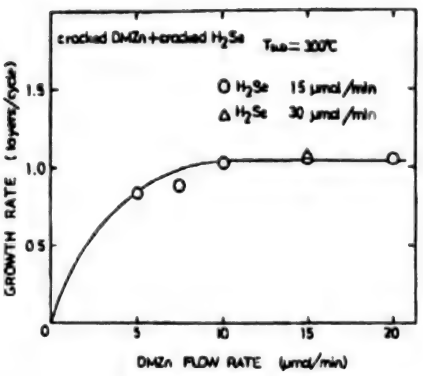

Figure 2. DMZn Supply Content Dependence of Growth Rate

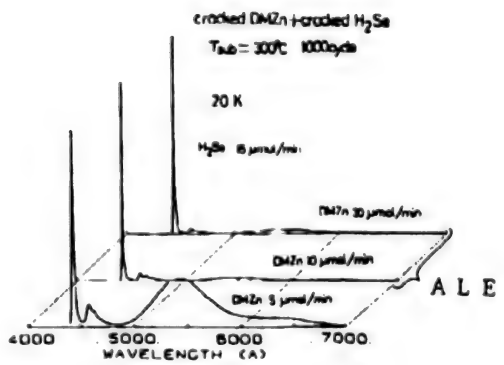

Figure 3. DMZn Supply Content Dependence of PL Spectrum

Measurement of the PL spectrum was then conducted to evaluate the film quality of the ALE-grown ZnSe thin film. Figure 3 shows the DMZn supply content dependence of the PL substrate at the substrate temperature of 300°C. Thin film with a DMZn supply content of 5 μmol/min did not attain ALE growth due to a DMZn supply deficiency, but thin film with a DMZn supply content of more than 10 μmol/min did demonstrate ALE growth. These samples were prepared by supplying materials in 1,000 cycles, and the film thickness was about 3000 A. In contrast to the luminescence on the exciton being dominant in a sample when the supply content is sufficient, i.e., in a sample with ALE growth, the luminescence from the deep level is strong in the sample with insufficient supply content, i.e., in a sample without ALE growth. In other words, the crystallinity is improved by A. In addition, it has been ascertained that the PL characteristics experienced practically no change when the supply content of DMZn in the sample was increased with ALE growth.

Since ALE growth is made by each single atomic layer that forms a film, it is expected that the surface will become extremely flat. Therefore, a surface morphology observation was conducted on the ZnSe thin film prepared by the ALE method. In addition, a sample of about the same film thickness was prepared by simultaneously supplying DMZn and H_2Se to provide a comparison, and a morphology observation was also conducted on its surface. The Normarski images of the thin films prepared by the ALE method and of those prepared by simultaneous supply are shown in Figure 4 [not reproduced]. It can be ascertained from this diagram that the thin film prepared by the ALE method excels in flatness and is extremely advantageous for superlattice production, etc.

4. When Cracking of Both Materials Is Not Conducted

ALE growth was undertaken without cracking the materials in an attempt to achieve chemical vapor depositional atomic layer growth by the chemical reaction of DMZn and H_2Se. In order to investigate the growth mechanism in this case in more detail, studies were made not only when neither material was cracked, but also when either DMZn or H_2Se was cracked.

The substrate temperature dependence of the growth rate when neither material was cracked and when DMZn only was cracked is shown in Figure 5. The amount of material supplied in this case is the same as that when both materials were cracked. It is clear from observing the diagram that the growth rate is slow, and ALE growth has not been attained in either case. However, it should be noted in this diagram that the substrate temperature dependence for no cracking almost coincides with that when DMZn only has been cracked. It can be ascertained from this fact that these reactions are not dependent on DMZn cracking, and that the rate-determination is made by H_2Se. In addition, the growth rate decreases with a rise in the substrate temperature in Figure 5, and this is thought to be due to the attachment coefficient reduction of H_2Se by the substrate temperature rise. Therefore, the reason for the growth rate being slow here is thought to be due to the attachment coefficient of H_2Se being quite small, and the supply amount is still insufficient compared to that when cracking has occurred.

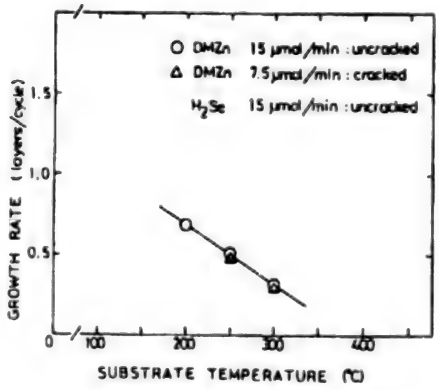

Figure 5. Substrate Temperature Dependence of Growth Rate

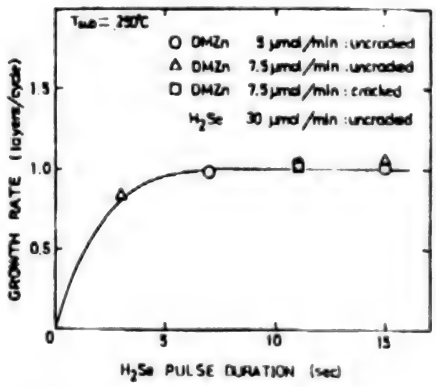

Figure 6. H_2Se Pulse Time Dependence of Growth Rate

ALE growth was attempted by changing the feed time of H_2Se in order to check the H_2Se supply content dependence of the growth rate. The H_2Se pulse time dependence of the growth speed at the substrate temperature of 250°C when no cracking occurs or with DMZn cracking only is shown in Figure 6. The feed pulse time and purge time in this case are 3 seconds and 5 seconds, respectively. It is ascertained from this diagram that the growth rate becomes saturated at a single molecular layer per cycle, even when the feed time of H_2Se is increased and the feed content per cycle is increased, and atomic layer growth can be realized without cracking the materials. However, the attachment coefficient becomes extremely small when cracking of H_2Se does not occur, and the supply content of H_2Se must be extremely great when conducting ALE growth without cracking.

Since the gas raw material reaches the substrate without decomposing if cracking does not occur, we must assume it is due to a new growth mechanism which is different from ALE growth involving the conventional MBE type growth. Therefore, ALE growth involving H_2Se cracking only was also attempted in studying the growth mechanism. The substrate temperature dependence of the growth rate when H_2Se only is cracked is shown in Figure 7. As mentioned previously, it is necessary to consider the relationship of the attachment

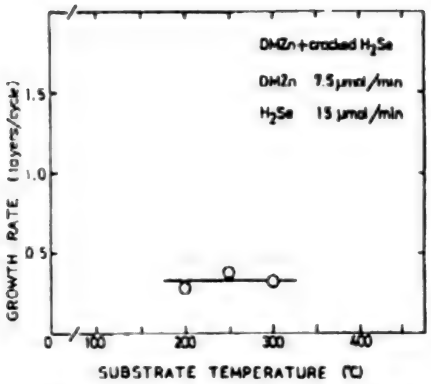

Figure 7. Substrate Temperature Dependence of Growth Rate

coefficient of the material gas to the substrate temperature and to make the supply content sufficient to realize ALE growth. Therefore, growth was conducted by supplying sufficient DMZn and H_2Se for ALE growth upon taking into consideration the results when cracking and not cracking both materials. Nevertheless, the growth rate was slow, and the ALE growth shown in Figure 7 did not occur. The following growth mechanism was studied from these results. Differing from normal depressured MOCVD, the reaction during the gas phase in MOMBE is negligible when cracking is not conducted. Therefore, materials either decompose independently on the substrate surface or adhere to the substrate in a molecular state. When assuming that the DMZn has decomposed independently on the substrate surface, an equivalent growth as that occurring when cracking both materials will occur when H_2Se only is cracked. Therefore, it can be expected that ALE growth will occur when H_2Se only is cracked, since ALE growth is realized when both materials are cracked. However, since the growth rate is slow and ALE growth does not occur when H_2Se only is cracked, it can be assumed that practically no independent decomposition of DMZn will occur on the substrate surface. Therefore, it can be concluded that in the growth mechanism, DMZn adheres to the substrate surface in the molecular state and forms a monomolecular layer, then decomposes by the chemical reaction with H_2Se and forms a ZnSe monomolecular layer. Since a chemical reaction with H_2Se is a requisite for DMZn decomposition in this case, it is believed that DMZn cannot be decomposed when H_2Se has been cracked, and the growth rate will become extremely slow.

The Normarski image of ALE growth thin film without cracking is shown in Figure 8 [not reproduced]. It is clear from this figure that the surface is extremely rough in comparison to that when both materials have been cracked (Figure 4 [not reproduced]). Since, in ALE growth as well, the materials adhere to the substrate surface in the molecular state and growth occurs due to the chemical reaction on the surface when cracking is not conducted, it is thought that sufficient migration cannot be made and the surface flatness will deteriorate.

A typical PL spectrum when material cracking is not conducted is shown in Figure 9. It is ascertained from this diagram that luminescence becomes dominant from the deep level when cracking is not conducted, and the film quality is extremely bad. It is also believed that crystallinity has become

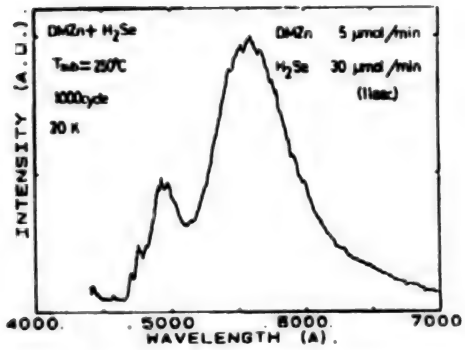

Figure 9. Typical PL Spectrum When Material Cracking Is Not Conducted

bad due to the surface reaction determining the growth rate, similar to the findings of the study made on surface morphology mentioned above.

5. Conclusion

The ALE growth of ZnSe has been attempted by the MOMBE method using DMZn and H_2Se as materials. As a result, it has become clear that ALE growth is realizable at a substrate temperature of 200~300°C by conducting cracking of both materials, and a high quality film is available. Specifically, it has been ascertained that the surface is superior in flatness and extremely advantageous for superlattice manufacture. In addition, it has been ascertained that ALE growth can also be realized when cracking is not conducted. Materials adhere in the molecular state to the substrate surface in this case, and growth results from their chemical reaction on the substrate surface. However, it has also become clear that the film quality deteriorates significantly due to the growth mechanism.

Note of Appreciation

We express our thanks to the Ministry of Education for aiding a portion of this research by means of a government subsidy for aiding scientific research.

References

1. Suntola, T., et al., U.S. Patent 4,058,430, 1977, and Japanese Patent 1147355, 1983.

2. Nishizawa, J., et al., "Extended Abstracts of the 16th Conf. on Solid State Devices and Materials," Kobe, Japan, 1984, p 1.

3. Doi, A., et al., APPL. PHYS. LETT., Vol 48, 1986 p 1787.

4. Usui, A., et al., JPN. J. APPL. PHYS., Vol 25, 1986, p L212.

5. Yao, T., et al., APPL. PHYS. LETT., Vol 48, 1986, p 160.

6. Ibid., JPN. J. APPL. PHYS., Vol 25, 1986, p L544.

7. Konagai, M., et al., "NATO Advanced Research Workshop on Growth and Optical Properties of Wire Gap II-VI's Low Dimensional Semiconductors," Regensburg, West Germany, 2-5 August 1988.

8. Yoshikawa, A., et al., J. CRYST. GROWTH, Vol 95, 1985, p 572.

Preparation of ZnSe-ZnS Perfect Superlattice on GaAs by Metallo-Organic Molecular Beam Epitaxy

43067199H Tokyo MES'89 in Japanese 17-18 Jul 89 pp 188-191

[Article by Hideyuki Oniyama, et al., Chiba University]

[Text] ZnSe, that is promising as a blue luminescence device material, generally grows on GaAs, but a misfit dislocation is generated by the lattice mismatching of ZnSe and GaAs, and this poses a serious problem involving its application to a device. The growth of a ZnSe-ZnS complete superlattice was attempted on GaAs to solve this problem. Confirmation that it was a perfect superlattice was given by the peak shift of photoluminescence and the film thickness dependence of the peak position and, moreover, it was clarified that the dislocation generation was held down by observing the EBIC image.

1. Introduction

ZnSe is a direct transition-type semiconductor with a forbidden bandwidth of 2.67 eV, equivalent to the blue color area, and its application to high efficiency blue light emission diodes and short wavelength lasers is expected. Since a good quality ZnSe bulk crystal is available when ZnSe is grown, GaAs with relatively small lattice mismatching (0.27 percent) is used as the substrate. However, it has now become possible to obtain high quality ZnSe by molecular beam epitaxy (MBE)[1] and metallo-organic vapor phase epitaxy (MOVPE)[2] methods and, with the valence electron controls such as the acceptor impurity addition, etc., being attempted, GaAs substrate and lattice mismatching no longer represent an important problem.[4] The situation shown in Figure 1 is reached when growing ZnSe on GaAs. The ZnSe lattice is subject to elastic deformation during the initial growth stage, and growth occurs so that the interfacial direction lattice constant coincides with the lattice constant of the GaAs substrate (coherent growth). However, the ZnSe lattice introduces dislocation and generates plastic deformation when exceeding a certain film thickness (about 1500 A).[5] The so-called misfit dislocation generated in such a manner forms at a deep level and exerts ill effects both optically and electrically, such as working as a trap against the carrier, etc.

Matching of the lattice to the GaAs substrate has been attempted by the ZnS_xSe_{1-x} mixed crystal (x=0.6 at RT) in order to solve this problem.[6] It is also possible to hold down the introduction of misfit dislocation by giving it

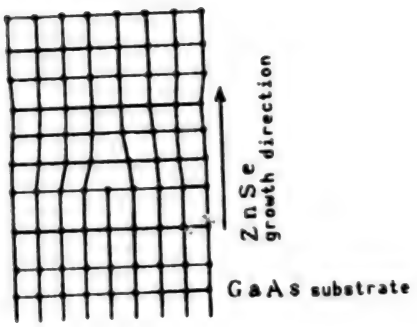

Figure 1. Lattice Deformation Model of ZnSe Epitaxial Film

a ZnSe–ZnS strain superlattice structure. In a strain superlattice consisting of ZnSe and ZnS, ZnSe with a large lattice constant receives two-dimensional compressive stress and the lattice shrinks in the interfacial direction as shown in Figure 2, and inversely, ZnS with a small lattice constant is pulled two-dimensionally and deforms by extending. When each layer of ZnSe and ZnS is sufficiently thin, the layers will be mutually balanced in the strained condition without generating a dislocation, and growth will be made with a certain average lattice constant. Since this average lattice constant is controllable by changing the thickness of each layer (d_{ZnSe}, d_{ZnS}), it is possible to grow the so-called perfect superlattice] which conducts lattice mismatching on the GaAs substrate.

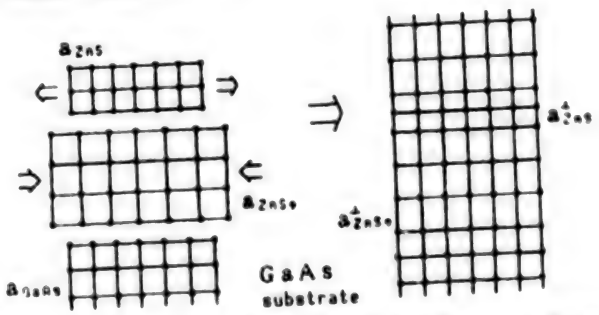

Figure 2. Lattice Model of ZnSe–Zn Strain Superlattice

We have paid attention to this characteristic and have attempted to grow a ZnSe–ZnS perfect superlattice by the metallo-organic molecular beam epitaxy (MOMBE) method[7-8] in which high quality ZnSe and ZnS crystals, excelling in film thickness controllability, etc., are available. A report of the results of this attempt will be made. In this research, the growth of a perfect superlattice was attempted in addition to studying conditions in which high quality strain superlattices are available. In addition, photoluminescence was used in a study on strain within the superlattice when lattice matching was made on the GaAs substrate.

Furthermore, an observation of superlattice layer dislocation has been attempted by the electron beam induced current (EBIC) method, and brief explanations of the results will be given.

2. Experiment

An outline of the MOMBE device used in the preparation of the ZnSe-ZnS strain superlattice is shown in Figure 3. The turbo-molecular pump is used as the main pump, back pressure after baking is about 10^{-8} Torr and the pressure at growth is 10^{-4}~10^{-8} Torr. DMZn, H_2Se and H_2S of 100 percent, respectively, were used as materials, and DMZn and H_2Se were supplied after cracking. The alternate growth of each ZnSe and ZnS layer was realized by controlling the air valve and shutter with a computer.

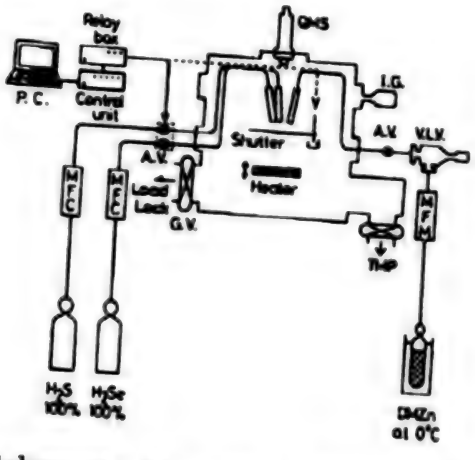

Figure 3. Schematic Diagram of Metallo-Organic Molecular Beam Epitaxy (MOMBE) Device

Semi-insulating (100) GaAs was used for the substrate and, after degreasing and etching by a sulfuric acid system etching reagent, it was boiled in HCl and installed in a chamber.

The n^+ ($n=1$~$4 \times 10^{18} cm^{-3}$) GaAs (100) was used for the substrate when the EBIC image was observed. After growth, about 500 A of gold was vacuum deposited on the sample surface, a Schottky electrode was formed and EBIC measurement was conducted. In addition, an InGa alloy was used for the ohmic electrode with the substrate.

3. Results and Discussions

Studies were first conducted regarding how the crystallinity changed with the superlattice structure. Explanations will first be made on this method. X-ray diffraction measurement was conducted on various samples with various layer thicknesses (d_{ZnSe}, d_{ZnS}), a simulation of the results was made by a computer based on the kinematical theory, and d_{ZnSe} and d_{ZnS} were obtained. An example of the simulation results of the X-ray diffraction pattern of a sample with 38 cycle growth at the substrate temperature of 330°C is shown in Figure 4. Satellite peaks of 0th, +1th, +2nd and -2nd are clear in the measured results. These satellite peaks coincide well in observation angle and diffraction strength with the theoretically obtained results, and it can be said that a high quality superlattice has been obtained. The film thickness of d_{ZnSe} and

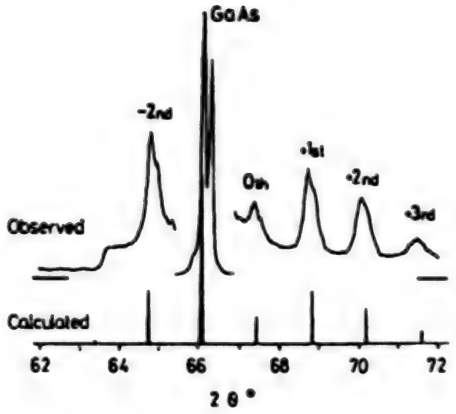

Figure 4. Simulation Results of X-Ray Diffraction Pattern

d_{ZnS} is 51.2 A and 26.7 A, respectively, as seen by the results shown in Figure 4. These values have been substituted in the following equation by Matthews, which gives the average lattice constant of the strain superlattice,[9] the average lattice constant a_{av}[11] was obtained, and the photoluminescence between this and GaAs was obtained.

$$a_{av}^{ii} = a_1 \left[1-f/(1 + G_1L_w/G_2L_b)\right] \quad (1)$$

However, $G_i = 2 \left[C_{11}^i + C_{12}^i - 2 (C_{11}^i)^2/C_{12}^i\right]$
C_{11}, C_{12}: Elastic constant
f: Lattice mismatch between ZnSe and ZnS

The results are shown in Figure 5. The film thickness of the ZnS layer of various samples is shown in the axis of abscissa, and the photoluminescence between GaAs and the average lattice constant is shown on the axis of ordinates in Figure 5. as a result of conducting X-ray diffraction on various samples, satellite peaks were separated into CuKal and Ka2, as shown in Figure 6(a). High quality samples are shown by (o) and broad samples like those in Figure 6(b) are shown by an x. It can be ascertained from this diagram that a high quality superlattice is available when the photoluminescence with the substrate is less than 1 percent or when the film thickness of the ZnS layer is less than 11 A.

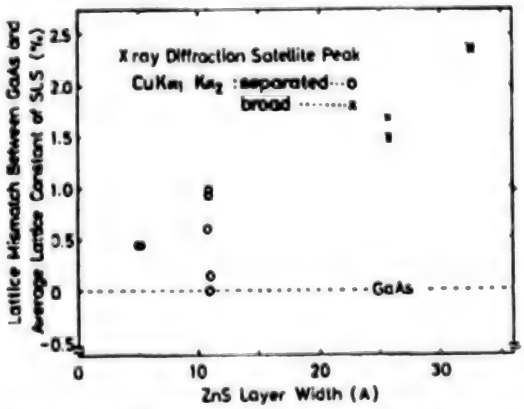

Figure 5. Lattice Mismatch Between Average Lattice Constant and GaAs of ZnSe-ZnS Strain Superlattice

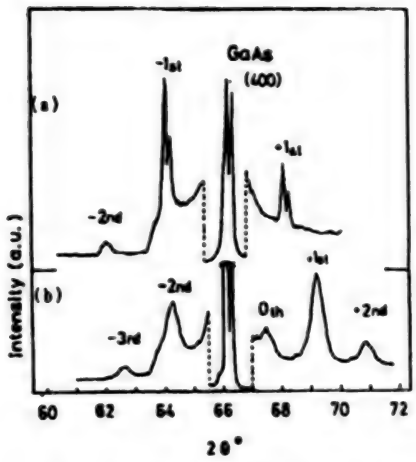

Figure 6. X-Ray Diffraction Pattern
(a) High quality superlattice
(b) Superlattice inferior in crystallinity

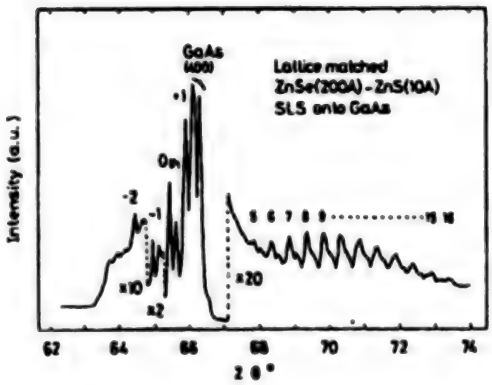

Figure 7. X-Ray Diffraction Pattern of Perfect Superlattice

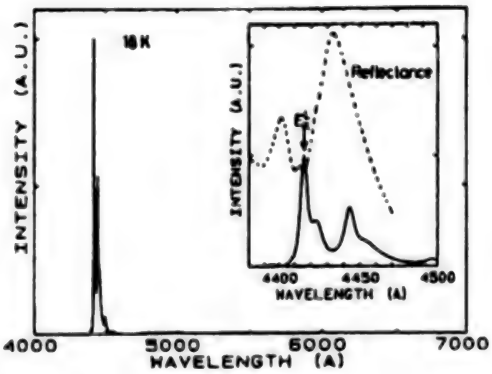

Figure 8. Photoluminescence Characteristics of Perfect Superlattice

The preparation of the so-called perfect superlattice for matching the lattice to the GaAs substrate was attempted by taking into account the results obtained above. According to equation (1), it will be all right to match the lattice to the substrate when the film thickness ratio between ZnS and ZnSe is 0.05. Therefore, the film thickness of each layer per cycle was made 200 A for the ZnSe layer and 10 A for the ZnS layer by taking into consideration the "ZnS layer thickness less than 11 A" mentioned above. The X-ray diffraction pattern and photoluminescence characteristics of a perfect superlattice of 25 cycles (film thickness of about 5000 A) with such a structure are shown in Figures 7 and 8, respectively. The peaks of Kal and Ka2 are clearly separated, despite the fact that a single cycle is large, at 210 A, and it is known that a superlattice with an interface excelling in flatness has been realized. In addition, the full width at half the luminescence maximum in the neighborhood of the band edge is extremely narrow, and about 9 meV, and luminescence from the deep level has become extremely weak, and it can be termed a high quality superlattice. It can be considered from the reflectance spectrum results, and

also since the ZnS layer that serves as the barrier layer in the superlattice of this system is thin and does not, for practical purposes, have a confinement effect on the carrier, that the band edge luminescence is free exciton luminescence in a strained ZnSe layer. It becomes 3.7 meV when obtaining the band gap change (Δ Eg) of ZnSe that results in strained lattice matching against GaAs[10] and, as a result, the free exciton luminescence shifts from 2.801 eV (4426 A) to 2.805 eV (4420 A) for bulk crystal. The free exciton luminescence appears at 4416 A in Figure 8, almost coinciding with the calculated value. These results confirm that the interface direction average lattice constant of the superlattice matches GaAs.

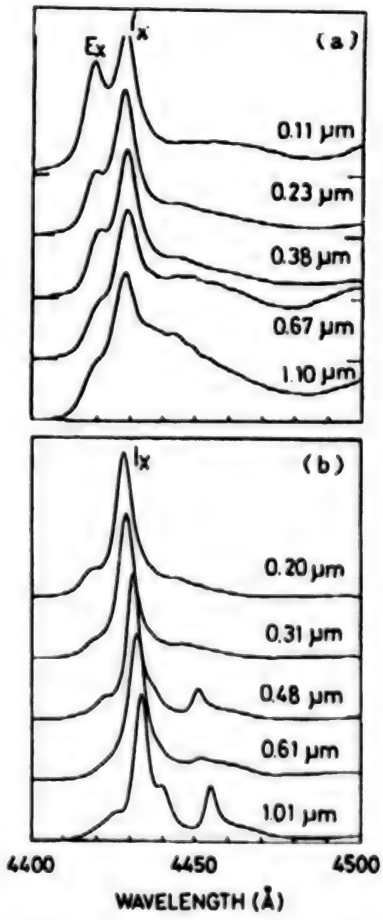

Figure 9. Thick Film Dependence of Photoluminescence Characteristic (a) Perfect superlattice; (b) ZnSe growth on GaAs; (E_x shows free exciton luminescence and I_x shows donor bound exciton luminescence.)

The film thickness dependence of photoluminescence on such a superlattice is shown in Figure 9(a), and, the film thickness dependence of ZnSe photoluminescence when ZnSe is grown on GaAs is shown in Figure 9(b). When a lattice mismatch between the substrate exists, as in ZnSe, the process occurs in which the superlattice strain relaxes from the coherent growth state due to the introduction of a dislocation and, therefore, the band gap changes

simultaneously, as does the luminescent peak position of photoluminescence, as shown in Figure 9(a). In contrast, a change in the exciton emission beam position is not recognized for the superlattice. This shows that there is no superlattice relaxation process, like that in ZnSe, and it is also known from this that lattice matching to GaAs has been made.

Lastly, a dislocation observation has been attempted by the EBIC method to confirm whether the dislocation generation was actually held down during the strain superlattice match to such a growth rate, and explanations of the results will be given. The EBIC image of ZnSe growth on GaAs is shown in Figure 10(b) [not reproduced]. A dislocation image is observed along the <100> direction. This is thought to be a dislocation related to the misfit dislocation according to reference 11, and it is clear that a misfit dislocation has been generated. In contrast, an image similar to that shown in Figure 10(b) [not reproduced] is not observed in the latticed matched superlattice shown in Figure 10 [not reproduced], and it is believed that the misfit location generation has been held down.

4. Conclusion

The growth of ZnSe-ZnS strain superlattice that is lattice matched with GaAs was attempted by metallo-organic molecular beam epitaxy (MOMBE). As a result of conducting studies on what sort of structure would be necessary to obtain a high quality superlattice when conducting growth on GaAs, it was ascertained that high quality was achieved when the ZnS layer was less than 11 A. Since the layer thickness ratio of ZnS and ZnSe becomes 0.05 when obtaining the structure that conducts lattice matching with GaAs according to Matthews' equation, superlattice growth with a ZnSe 200 A and ZnS 10 A structure was conducted by taking the above results into account. It was confirmed that the so-called perfect superlattice, in which the lattice was matched with GaAs, was available from the luminous peak shift during photoluminescence and from the film thickness dependence of the luminous peak position. In addition, by observing the EBIC image, it was ascertained that dislocation generation was actually held down. Problems involving device manufacturing were solved by means of the above results, and it can be said that the basis has been established for attempting to add impurities to ZnSe-ZnS perfect superlattices and for controlling the conduction type and conductivity in the future.

Note of Appreciation

We express our thanks to the Ministry of Education for aiding a portion of this research by means of a government subsidy for aiding scientific research.

References

1. Yao, T. and Maekawa, S., J. CRYSTAL GROWTH, Vol 53, 1981, P 423.

2. Kamata, A., Hirahara, K., Kawachi, M. and Beppu, T., "Abstracts 17th Conf. on Solid State Devices and Materials," Tokyo, 1985, p 233.

3. Yoshikawa, A., Yamaga, S. and Tanaka, K., JPN. J. APPL. PHYS., Vol 23, 1984, p L388.

4. Fujita, Sz., Terada, K., Sakamoto, T. and Fujita, Sg., J. CRYSTAL GROWTH, Vol 94, 1989, p 102.

5. Mitsuhasahi, H., Mitsuishi, I., Mizuta, M. and Kukimoto, H., JPN. J. APPL. PHYS., Vol 24, 1985, p L578.

6. Matsumura, N., Ishikawa, K., Saraie, J. and Yodogawa, Y., J. CRYSTAL GROWTH, Vol 72, 1985, p 41.

7. Oniyama, H., Yamaga, S., Yoshikawa, A. and Kasai, H., Ibid., Vol 93, 1988, p 679.

8. Yoshikawa, A., Oniyama, H., Yamaga, S. and Kasai, H., Ibid., Vol 95, 1989, p 572.

9. Matthews, J.W. and Blakeslee, A.E., Ibid., Vol 32, 1976, p 265.

10. Kawakami, Y., Taguchi, T. and Hiraki, A., Ibid., Vol 93, 1988, p 714.

11. Shinohara, M., Ito, T., Yamada, K. and Imamura, Y., JPN. J. APPL. PHYS., Vol 24, 1985, p L818.

Formation of Thin Film Reservoir by Metallo-Organic Deposition Method

43067199I Tokyo MES'89 in Japanese 17-18 Jul 89 pp 196-199

[Article by Kazuo Baba, et al., Fuji Xerox Co., Ltd.]

[Text] The formation of an oxide thin film resistor was studied for the purpose of obtaining a thin and homogeneous thermal head exothermic resistor by a thick film process. A thin film resistor with a wide sheet resistance range of 30 Ω/aperture~20 kΩ/aperture and excelling in both electrical and printing characteristics has been obtained by applying and baking a metallo-organic substance solution consisting of platinum group elements that become glass components.

1. Introduction

The dissemination of information equipment, such as facsimiles, work stations, etc., in offices has been remarkable. Printers that output information have also spread widely, and the main current has moved from impact printers, such as dot matrix printing, etc., to nonimpact printers, such as laser, ink jet and thermal printing. Since, of the nonimpact printers, thermal printing involves a simple mechanism, maintenance is easy and the device can be made compact at a low price, its development has been particularly noted, centering around its facsimile application.

Thermal printing employs a thermal head as its key device, which can be largely classified into thin and thick film types according to the method of preparation. The thick film type excels in productivity and is low in cost, however, its problems include being inferior in image quality to the thin film type. Therefore, the high performance realization of the thick film type has been promoted by attempting to solve these problems through resistance value adjustment technology by means of the high pressure pulse trimming method[1] and resistor shape control technology by means of the liftoff method.[2] However, a thinner and more homogeneous resistor, similar to that used in the thin film type, which will be capable of conducting etching for promoting the realization of a high resolution of more than 12 dots/mm and the resistance alue homogeneity demanded in the sublimation type color transfer printing, etc., must be developed.

For this reason, we initiated research on a thin film resistor forming technology by the MOD (metallo-organic deposition) method. MOD obtains a thin film by the same process as that used for the conventional thick film but, while the conventional thick film method sinters a micron order powder, the MOD method sinters the metallic elements at the atomic level by utilizing the thermal decomposition of metallo-organic substances.

In this research, the forming of thin films in which platinum group elements and oxides comprise the main components, the film characteristics and the performance of the thermal head using this resistance film have been studied.

2. Formation and Analysis of MOD Thin Film

2.1 Formation Process

The metallo-organic substance solution (metal resinite) on the market and synthesized carboxylic complex were used as the metallo-organic substance materials.

Two to five types of metallo-organic substance solutions of platinum group elements (Ru, Ir, Rh) and metallo-organic substance solutions of elements in which oxides became the glass component were mixed so that the metallic elements were in the prescribed atomic number ratio, and viscosity was adjusted to 8×10^3~2×10^4cP due to the addition of resins, such as ethyl cellulose, etc. This solution was printed and applied on the alumina substrate glaze by a 150~400 mesh screen and, after drying, it was baked for 6~16 minutes at a peak temperature of 600~900°C by means of an infrared belt furnace.

2.2 Composition and Characteristics

Attention was first given to ruthenium oxide (RuO_2) that was generally used in the thick film-type thermal head, and independent film formation by ruthenium resinite was attempted during the film forming experiment. However, since the film forming properties of the ruthenium resinite were extremely bad, silicon (Si), generating silicon dioxide (SiO_2), a glass component, was selected along with barium (Ba), since barium ruthenite ($BaRuO_3$) is used in thin type resistors,[4] and film forming was attempted by making it a two component system, respectively, with Ru. The result was that although it did not become a continuous film in the Ru/Ba system, a continuous film was obtained in the Ru/Si system, although adhesion with the substrate was low.

Therefore, bismuth (Bi), known as able to form a component with RuO_2, or lead (Pb) was added, and a three component system was made to improve the film adhesion of the Ru/Si system. As a result, a homogeneous film without pinholes and cracks was obtained, and adhesion was sufficient for practical use in both systems. The film thickness was 0.25 μm when using the 400 mesh screen and the sheet resistance was about 80 Ω/aperture. This sheet resistance is somewhat low for the thermal head resistor.

Next, two methods of 1) adding a fourth metal component and 2) using iridium (Ir) or rhodium (Rh) in place of Ru were attempted to obtain a film with a sheet resistance of 200 Ω/aperture~2 kΩ/aperture, which was appropriate for the thermal head.

As a result of adding aluminum (Al), boron (B), titanium (Ti), zirconium (Zr) and calcium (Ca) that produced oxides which became glass components in the former method, a film with a sheet resistance of 30 Ω/aperture~1.1 kΩ/aperture was obtained according to types and component ratios, but condensates were generated in the films with a high resistance.

A film with good surface properties and a wide range sheet resistance of 130 Ω/aperture~20 kΩ/aperture was obtained by the latter method.

The sheet resistance range of the respective systems of Ru, Ir and Rh of the platinum group elements is shown in Figure 1. The relative size of this sheet resistance coincides with the relative size of specific resistance[5] that has been reported on the Ru, Ir and Rh oxides, respectively, and it is assumed that the platinum group elements contribute to the electroconductivity of the MOD resistor films.

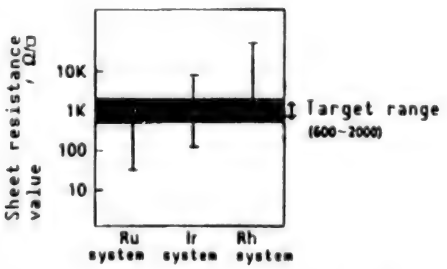

Figure 1. Platinum Group Oxides and Sheet Resistance Range

2.3 Structural Analysis

Measurement was made by X-ray diffraction for checking the crystal structure of MOD resistor films. The Cu;Ka ray (λ=0.15406 nm) was used for the X-ray source. The measurement results of the 800°C baked sample of the Ru/Si/bi system are shown together with the data of the ruthenium oxide system thick film resistor in Figure 2. Only the RuO_2 diffraction peak of the rutile type appears in both the MOD resistor film and thick film resistor. Neither Si nor Bi has crystallized, and it is thought that an amorphous substance (glassy state) exists. In addition, no $Bi_2Ru_2O_7$, a pyrochlore system electroconductive compound oxide, was observed. The same was true in the Ir/Si/Bi system, with the result that IrO_2 was the only one crystallized.

The relationship between the baking temperature and crystallinity in the Ir/Si/Bi/Ca system is shown in Figure 3. The baking temperature ranges from 500~900°C, and the IrO_2 diffraction peak appears at more than 600°C. The diffraction peak becomes sharp and crystallinity is improved as the baking temperature rises, but the changes occurring at more than 700°C are small.

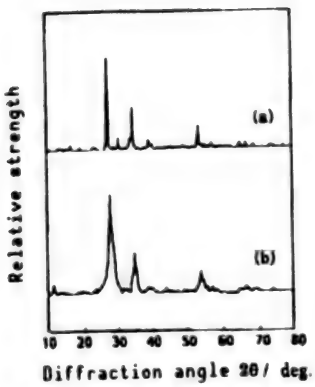

Figure 2. X-Ray Diffraction Pattern
(a) Thick film resistor (RuO_2)
(b) MOD resistor (Ru/Si/Bi)

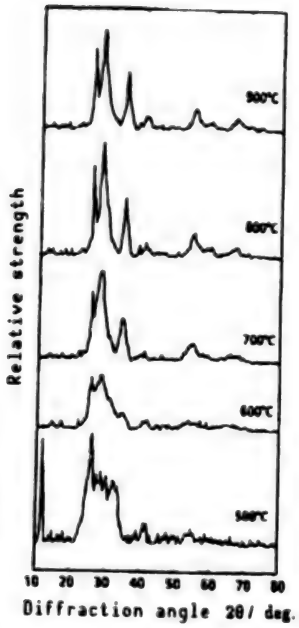

Figure 3. Temperature Dependence of of X-Ray Diffraction Pattern (Ir/Si/Bi/Ca)

In addition, as a result of investigating the depth direction element concentration distribution of the Ir/Si/Bi system MOD resistor film by Auger electron spectroanalysis, it was ascertained that, although Si was homogeneously distributed on the film, the Ir in the film was gradually reduced, beginning in the middle and extending toward the depth direction.

3. Application to Thermal Head

3.1 Preparation of Strip Thermal Head

A strip thermal head with 288 dots and a density of 8-24 dots/mm was prepared by using the Ir/Si/Bi/Zr system resistor film that was formed by the MOD method.

First of all, a resistor is formed on the alumina substrate glaze by the method mentioned in the preceding section. Then, an organic gold paste is printed and baked so as to cover the resistor film, and a gold film is formed by the same MOD method as that used for the resistor. This gold film is subjected to photolithographic etching by using iodine and potassium iodine solution as the etching agents, and an electrode pattern is formed. Then, photolithographic etching is conducted, with the electrode pattern as the mask, by using a mixed solution of hydrofluoric acid and nitric acid as the etching agents. Since a gold film is actually on the resistor part that is to be heated under these conditions, this portion of the metal film is removed by photolithographic etching and a heat generating part is formed. Lastly, the overglaze layer is laminated by printing and baking of ordinary thick film glass paste.

3.2 Characteristic Evaluation

An evaluation of the resistance value, resistance value dispersion, electric power resistance strength by the step-up stress test (SST), electric field resistance strength by condenser discharge, temperature coefficient of resistance (TCR) and printing has been conducted for the trial-manufactured strip thermal head.

(1) Resistance Value and Resistance Value Dispersion

The measured resistance values for the thick film thermal head with a total of 288 dots at 8 dots/mm and MOD thermal head are shown in Figure 4. The relative standard deviation of the MOD resistor is 3.1 percent for the resistance value dispersion within the substrate, which is important from the standpoint of printing quality and is small in comparison to the conventional thick film resistor. It has been reduced considerably to 2.5 percent in the MOD resistor, in contrast to the resistance value difference among neighboring dots which is more than 20 percent for the thick film resistor. The same results were also obtained on the thermal head with more than 12 dots/mm.

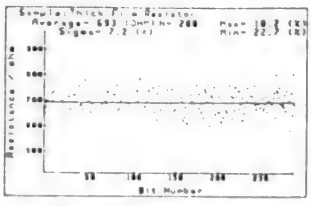

(a) Thick film resistor

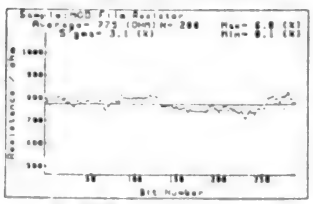

(b) MOD resistor

Figure 4. Measured Resistance Values
(8 dots/mm, 288 dots)

The average resistance value of the MOD resistor can be easily adjusted from 100 Ω to about 3 kΩ by changing the type and ratio of the mixing materials.

(2) Electric Power Resistance Strength

The electric power resistance strength and resistance value stability were investigated by the step-up stress test (SST). The conditions of the SST were an applied pulse width of 1 msec, cycle of 10 msec, applied pulse frequency of 1000 pulses, and step-up was made at the pitch of 0.1 W/dot from 0.1 W/dot.

The results of the SST are shown with the thick film resistor results in Figure 5. The electric power at which the resistance value of the MOD resistor starts to rise is about 10-20 percent greater than that of the thick

film resistor. Moreover, the resistance value change of the MOD resistor is slower than that of the thick film resistor, and it is stable as a resistor material.

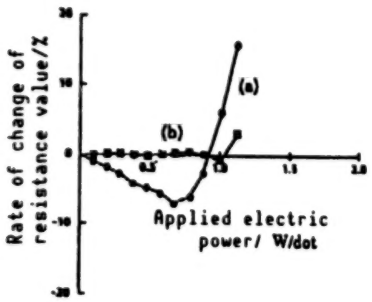

Figure 5. Step-Up Stress Test Results
(a) Thick film resistor
(b) MOD resistor

(3) Electric Field Resistance Strength

It is known that the resistance value of the thick film resistor changes greatly due to static electricity. Therefore, a surge was applied to the resistor by discharging the electric charge stored in the condenser for about 40 nsec, the resistance value was measured before and after the surge and the strength against the electric field was checked.

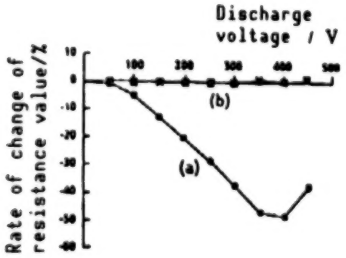

Figure 6. Condenser Discharge Test Results
(a) Thick film resistor
(b) MOD resistor

Measurement results are shown in Figure 6. Although the resistance value of the thick film resistor reduced almost in proportion to the applied voltage, the resistance value of the MOD resistor did not change up to the upper limit measured of 500 V. This shows that the MOD resistor has high reliability against electrical noises and static electricity.

(4) Temperature Coefficient of Resistance (TCR)

TCR measurement was obtained by placing a sample on a hot plate and measuring the dot resistance value from room temperature to about 200°C.

While the conventional ruthenium oxide system thick film resistor reaches about -200 ppm/°C, the results showed that the MOD resistor value becomes

±30 ppm/°C, which is quite small. In addition, since the MOD resistor exhibited negative characteristics up to about 100°C and positive characteristics at temperatures above 100°C, it is believed that it has an electroconductive mechanism with both semiconductor-like and metallic parts.

(5) Printing Characteristics

Printing characteristics can be largely classified into printing energy and printing quality. There were no differences in printing energy between the conventional thick film resistor and thin film resistor, and this was also the case for the MOD resistor.

(a) Thick film resistor (b) MOD resistor

Figure 7. Printing Samples
(8 dots/mm, 24 x 24 dots)

As seen in the enlarged photo of the printed part shown in Figure 7, the dots are rectangular and linkage is good in the head of the MOD method in contrast to the printing quality of the thick film resistor, which demonstrates a bad linkage of the printed dots. This is thought to be due to the resistor of the MOD method having superior thermal separation. The printed dots become rectangular by reproducing the resistor shape since each dot is individually separated, while with the thick film resistor, since it adopts a belt-like structure, there is a large dispersion of printed dot sizes.

4. Conclusion

A thin film resistor with platinum group oxides as the main components was formed by the MOD method by using metallo-organic substances. This thin film resistor demonstrates superior characteristics as a thermal head resistor. The significant characteristics are 1) the resistance value can vary within a wide range by changing the composition, 2) fine patterns are made by photoluminescence etching, 3) the resistance value dispersion and resistance value difference among neighboring dots are small, and 4) the electric power resistance strength and electric field resistance strength are great.

The evaluation results of the MOD resistor mentioned in this report demonstrate, as mentioned above, that the resistor has characteristics that far surpass those of conventional thick film resistors when used as a thermal head resistor in which high resolution and high picture quality are demanded, and that it can also be applied effectively as an HIC resistor.

References

1. Tobita, T., et al., "Advanced Thick-Film Techniques Applied for a New Type Printing Head," ISHM PROC., 1985, pp 494-499.

2. Yamaguchi, Y., et al., "Realization of High Picture Quality of Thick Film Thermal Head by Individual Separation Resistor Formation Technology," Study Meeting Manuscript of Image Electron Society, 87-05, 1988, pp 31-36.

3. Kuo, C.Y., "Electrical Applications of Thin-Films Produced by Metallo-Organic Deposition," SOLID STATE TECHNOLOGY, 1974, pp 49-55.

4. Takikawa, O., et al., "A New $BaRuO_3$ Thin Film Resistor for High Speed Thermal Printing," IEEE CHMT-9, 1986, pp 214-218.

5. Tsuda, T., "Electroconductive Oxides," Shokabo, 1983.

END OF FICHE

DATE FILMED

7 MAY 90